# Annual Report



## Studies on Equatorial Shock Formation During Plasmaspheric Refilling

Grant # NAGW-2128
P.I.: Dr. N. Singh

During the grant period starting August 1, 1992, our major effort has been on examining the presence of equatorially trapped hot plasma on plasmaspheric refilling. We performed one-dimensional PIC simulations of cold plasmas expanding into a hot plasma, consisting of hot anisotropic ions and warm isotropic electrons, trapped in a region of minimum magnetic field. Simulations showed that the electric potential barrier built up by the anisotropy of the hot ion population facilitates in the formation of electrostatic shocks when the cold ion beams begin to come into contact with the hot plasma. The shock formation occurs even when the cold ion beams are highly supersonic with respect to the ion-acoustic speed. This finding is interesting because equatorial shock formation during the early stage of plasmaspheric refilling has been debated over about two decades. In the past ion-ion instability has been invoked as the main mechanism for the coupling between the cold ion beams approaching the equator from the conjugate ionspheres. This coupling occurs when the beams are sufficiently slow; the beam velocity being less than three times the ion-acoustic speed. In the presence of hot plasma, the beams slow down by the potential barrier. The slowing down and the reflection process lead to the formation of the electrostatic shock even for highly supersonic ion beams.

The mixing of hot and cold plasma was also studied. It was found that the cold electrons eventually short-circuit the potential barrier and the cold plasma punches through the equatorially trapped hot plasma. This spatial mixing produces velocity distribution functions which are potentially unstable. The perpendicular velocity distribution of ions consists of a cold core and a hot ring; the latter starts at the ion energy corresponding to the magnitude of the initial potential barrier set up by the plasma. Such ring distributions are known to be unstable exciting ion-Bernstein modes, as well as lower hybrid waves. These waves can in turn heat the cold core.

The results from this study were reported in a Huntsville Workshop (October 15-17, 1992) on plasma models, AGU 1992 Fall meeting [Singh, 1992] and a paper written for Geophysical Research letters [Singh, 1993]. An extended paper for JGR is under preparation.

During this grant period we have also continued our investigation of the comparison of the large-scale hydrodynamic and kinetic models for plasmaspheric refilling. comparison brings out the shortcomings and the strengths of the respective models [Singh, 1993]. This study also reconciles some of the previously reported results from these models.

## Recent Publications Under Grant # NAGW-2128


1. Lin, J., L. J. Horwitz, G. R. Wilson, C. W. Ho, and D. G. Brown, A semikinetic model for early state plasmaspheric refilling, 2, Effects of wave-particle interactions, *J. Geophys. Res.*, 97, 1121, 1992.

2. Singh, N., Interaction of field-aligned cold plasma flows with an equatorially-trapped hot plasma: electrostatic shock formation, *Geophys. Res.* letters, in press, 1993.

3. Singh, N., Numerical simulation of hot plasma effects on early plasmaspheric refilling (Abstract), *EOS*, 73, 479, 1992.

4. Singh, N., G. R. Wilson, and J. L. Horwitz, Comparison of hydrodynamic and semikinetic models for plasma flow along closed field lines (Abstract), *J. Geophys. Res.*, Submitted, 1993.

5. Singh, N., C. B. Chan, Effects of equatorially trapped ions on refilling of the outer palsmasphere, *J. Geophys. Res.*, 97, 1167, 1992.

6. Wilson, G. R., N. Singh and J. L. Horwitz, Comparison of hydrodynamic and semikinetic model for plasma flow along closed field lines (Abstract), *EOS*, 73, 479, 1992.

7. Wilson, G. R., J. L. Horwitz, and J. Lin, a semikinetic model for early-stage plasmaspheric refilling, 1, Effects of Coulomb collisions, *J. Geophys. Res.*, 97, 1109, 1992.

GEOPHYSICAL RESEARCH LETTERS, VOL. 20, NO. 9, PAGES 799-802, MAY 5, 1993

# INTERACTION OF FIELD-ALIGNED COLD PLASMA FLOWS WITH AN EQUATORIALLY-TRAPPED HOT PLASMA: ELECTROSTATIC SHOCK FORMATION

Nagendra Singh

Department of Electrical and Computer Engineering, University of Alabama in Huntsville

Abstract. Effects of equatorially trapped hot plasma on the highly supersonic cold-plasma flow occurring during early stage plasmaspheric refilling are studied by means of numerical simulations. It is shown that the equatorially trapped hot ions set up a potential barrier for the cold ion beams and facilitate formation of electrostatic shocks by reflecting them from the equatorial region. Simulations with and without the hot plasma show different flow properties; the formation of electrostatic shocks occur only in the former case. The simulation with the hot plasma also reveals that the magnetic trapping in conjunction with the evolution of the electrostatic potential barrier produces ion velocity distribution functions consisting of a cold core and a hot ring in the perpendicular velocity. Such a distribution function provides a source of free energy for equatorial waves. The corresponding electron population is warm and field aligned.

## Introduction

So far most theoretical studies on plasmaspheric refilling have been primarily concerned with the outflow of cold ionospheric plasma and its trapping in the flux tube. In such theoretical studies an important observational fact, which has been ignored, is that the flux tubes undergoing refilling contain a hot plasma population trapped in the equatorial region. Such plasmas originate from the ring current or the plasma sheet and are characterized by $T_{i\perp}^H > T_{i\|}^H$, where $T_{i\perp}^H$ and $T_{i\|}^H$ are the perpendicular and parallel temperatures of the hot ions, respectively. Specific observations of such hot ions having relatively large pitch angle anisotropies ($A_i = T_{i\perp}^H/T_{i\|}^H > 2$) come from GEOS-1 and -2, which observed the hot ions in the energy range > 10 keV in the noon sector. Such hot ions are known to excite electromagnetic ion cyclotron waves [ Roux et al., 1982].

Another set of observations, where the role of hot plasma has been invoked, deals with thermal ions transversely heated to energies up to a few hundred eV and trapped in the equatorial region [*Olsen et al.*, 1987]. Here again hot ions are suggested to be the source of free energy for exciting the broadband waves observed from DE-1. Theories suggest that the broadband waves are driven by a combined effect of temperature anisotropy and ring type of distributions of energetic protons [*Perraut et al.*, 1982 ]. The effect of heating of the thermal ions on refilling has been studied [*Singh and Chan*, 1992], but the direct effect of the hot ions on the refilling has not been studied so far.

The purpose of this letter is to show that the hot anisotropic ions, which are commonly present in the equatorial region of flux tubes undergoing refilling and drive the equatorial processes discussed above [*Olsen et al.*, 1987; *Roux et al.*, 1982], facilitate the process of electrostatic shock formation since they provide an effective potential barrier for the upflowing ion beams of cold ionospheric plasma. The shock formation occurs even for highly supersonic ion beams which are expected to occur during early stage refilling [*Banks et al.*, 1971; *Singh et al.*, 1986; *Rasmussen and Schunk*, 1988; *Singh*, 1990; *Wilson et al.*, 1992]. If the hot plasma consists of isotropic electrons and anisotropic biMaxwellian ions with anisotropy $A_i = T_{i\perp}^H/T_{i\|}^H > 1$, the potential difference between the equator, where the minimum magnetic field strength is $B_m$, and an ionospheric point where the magnetic field is $B$, is given by $\Phi = kT_{i\|}^H/e[1 + T_{i\|}^H/T_e]^{-1} \ln(\Gamma)$, where $\Gamma = A_i(1 - B_m/B) + B_m/B$ [*Whipple*, 1977].

Since $B_m/B << 1$, the equatorial potential with respect to the ionosphere for $T_e << T_{i\|}^H$ is $\Phi \simeq (kT_e/e)\ln(A_i)$. For $A_i = 2$ and $kT_e/e = 10$ V, the typical values for these parameters used in wave analysis [*Roux et al.*, 1982], $\Phi \simeq 7$ V. However, this potential difference is true when no ionospheric cold plasma is present; in the presence of a cold plasma, it is not certain how large the potential difference is and how it is distributed along the field line. In the following discussion, we present results from numerical simulations elucidating the interactions between cold and hot plasmas when the former plasma flows into the latter one trapped in a magnetic mirror. The simulation presented here is small scale, in contrast to the large-scale problem in space. Therefore, the results presented here only serve the purpose of elucidating the processes involved in hot-cold plasma interactions.

## Numerical Model

We perform a one-dimensional particle-in-cell simulation of plasma flow along an artificial flux tube (Figure 1a). The magnetic field $B(X) = B_0(1 - \alpha \exp[-(X - d/2)^2/\sigma^2])$ where $B_0$ is a constant field outside the minimum-field region, d is the size of the simulation system and the choice of $\alpha$ and $\sigma$ determines the desired field distribution. The hot plasma is created by injecting a large number of electrons and ions in the minimum-B field region. Such plasma particles are chosen from Maxwellian or bi-Maxwellian velocity distributions depending upon the requirement of a simulation run. The cold plasma flows into the flux tube from the two plasma reservoirs at



Paper number 93GL00492
0094-8534/93/93GL-00492$03.00

the ends of the simulation system at $X = 0$ and $X = d$ (Figure 1a). The simulation technique is described in *Singh and Chan* [1992]. We solve for the motions of charged particles in self-consistent electric fields, determined by solving Poisson's equation. As the particles move in the flux tube, their magnetic moments are assumed to be conserved.

In the cold-plasma reservoirs electron and ion temperatures are $T_0$. The reservoirs supply a continuous flux of charged particles into the flux tube through the process of plasma expansion. In the simulations reported here, we have used $m_i/m_e = 400$, which adequately separates the electron and ion time scales and, at the same time, allows computationally feasible runs. The hot plasma is injected into the central region of the simulation system at time t=0 (Figure 1a). The properties of the hot plasma are described later. Numerical parameters of the simulations are as follows: system size d = 5 $\times 10^3$ $\lambda_d$, $B$ field parameters $\alpha = 0.9$, $\sigma = 750$ $\lambda_d$, cell size $\Delta x = 20$ $\lambda_d$, and time step $\Delta t = 0.1\omega_{peo}^{-1}$, where $\lambda_d$ and $\omega_{peo}$ are the Debye length and electron-plasma frequency in the cold plasma reservoirs. In the following discussion we have used normalized quantities defined as follows: time $\bar{t} = t\omega_{pio}$, distance $\bar{X} = X/\lambda_d$, velocity $\bar{V} = V/V_{te}$ and electric potential $\bar{\Phi} = e\Phi/kT_0$, where $V_{te} = (kT_0/m_e)^{1/2}$ and $\omega_{pio} = (m_e/m_i)^{1/2}\omega_{peo}$.

## Numerical Results

First we present results from a simulation in which "equatorial" hot plasma is not included. This simulation serves as a reference against which the hot plasma effects on the cold plasma flow are compared. Figures 1b to 1f show the temporal evolution of the flow of cold ions into the flux tube from the reservoirs shown in Figure 1a. These panels show the phase-space plots in the $X - V_{||}$ plane. Each dot in the figure represents an ion, giving its parallel velocity and position. The simulation begins at t = 0, when plasmas from the reservoirs begin to flow

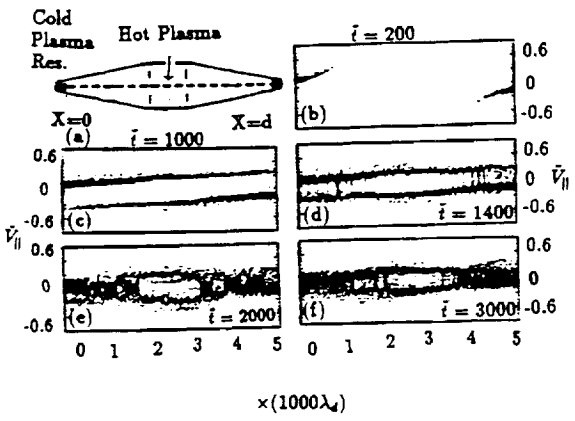


Fig. 1. (a) Artificial flux tube in which plasma expands from the cold plasma reservoirs at X=0 and X=d. The hot plasma is injected in the central region. (b) to (f) ion phase-space plots in $X - V_{||}$ plane at selected times as shown. The plots show evolution of the cold plasma flow in absence of a hot plasma.

in the flux tube. The corresponding flow of electrons is not shown here. Figure 1b shows expanding ion beams into the simulation region at $\bar{t} = 200$. The plot for $\bar{t} =$ 1,000 (Figure 1c) shows that the ion beams have expanded from one end to the other end of the simulation region, setting up counterstreaming. Equatorial shock formation has not occurred. At this time, ion beams are too fast to couple through the ion-ion instability; the relative flow velocity between the beams is $V_{rel} = 0.4V_{te} \simeq 8c_s$, where $c_s$ is the local ion-acoustic speed at the equator, X = d/2, and is about $.05V_{te}$. However, at later times the beams become progressively slower as the plasma accumulates in the flux tube, and when they become sufficiently slow in the regions near the ends of the flux tube they excite ion-ion instability as seen for $\bar{t} \geq$ 1,400 (Figures 1d to 1f); the instability creates vortex-like structures in the phase space.

The instability is seen to thermalize the ion beams (Figure 1e). However, in the middle of the simulation region, where the magnetic field is minimum, counterstreaming of ion beams is seen to persist.

Simulation with a hot plasma in the region of minimum magnetic field reveals a quite different behavior of the flow. We performed several simulations by varying the temperatures of the hot plasma but kept ion anisotropy $A_i > 1$ and electron anisotropy $A_e = 1$ and $T_e << T_{i||}^H$. Such properties of hot plasma have been measured [*Roux et al.*, 1982]. Relative densities of the cold ($n_C$) and hot ($n_H$) ions in their respective source regions were also varied. The results from such a parametric study will be reported elsewhere. We present results here for $T_{i||}^H = T_{i\perp}^H/2 = 900T_0$, $T_e = 10T_0$, and $n_C \simeq 100\ n_H$.

The hot plasma is injected in the central region $2300 \leq x/\lambda_d < 2700$ at t = 0, when cold plasma flows begin from the reservoirs. Figure 2 shows the evolution of the cold plasma flow along with the potential and density profiles in the flux tube. The panels a to d show the ion phase space plot in $X - V_{||}$ plane. The phase-space plot of ions in $X - V_\perp$ plane is shown in panels e to h. The evolution of the potential profiles in the flux tube is shown in panels i to l, and the corresponding plasma density is shown in panels m to p. The evolution of the electron phase-space ($X - V_{||}$) is shown in panels q to t. As shown on the top of the figure, the columns from left to right show the properties of the flow at $\bar{t} = 100$, 500, 700, and 1000, respectively. At an early time ($\bar{t} = 100$), the flow can be characterized by the following features: (1) expanding cold ion beams (panel a), (2) equatorially trapped ions originating from the hot plasma (panel e), (3) a potential maximum at the midpoint of the simulation region (panel i), and (4) a density maximum coinciding with the potential maximum (panel m). The density maximum at this time entirely represents the trapped hot ions, and there is no contribution from the cold plasma flow.

At $\bar{t} = 500$, the cold plasma flow comes into contact with the hot plasma; the cold ion beams have somewhat penetrated into the region of the hot plasma (panels b and f). Already the cold beams show the sign of retardation by the potential barrier. The slowing down of the ion beams enhances the potential barrier further; panel j shows that at $\bar{t} = 500$ the equatorial potential maximum has grown to $15kT_0/e$, in contrast to $3kT_0/e$ at $\bar{t} = 100$.

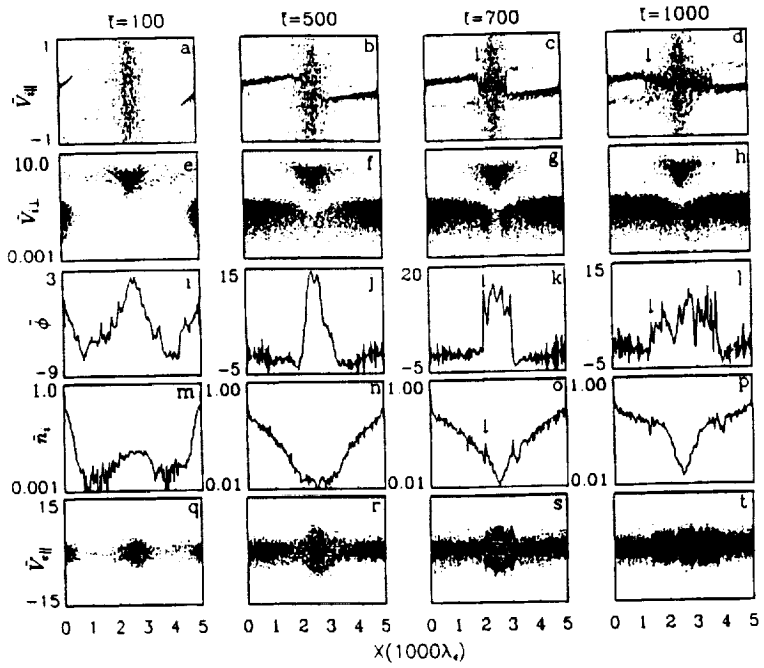


Fig. 2. Evolution of the cold plasma flow in the presence of equatorially trapped hot ions. Each column shows the state of the plasma at times shown at the top. (a) to (d) $X - V_{\parallel}$ phase-space plots for ions, (e) to (h) $X - V_{\perp}$ phase space plots for ion, (i) to (l) Potential distributions, (m) to (p) Ion density distributions, and (q) to (t) Electron phase-space plots in $X - V_{\parallel}$ plane.

Note the change in the vertical scale between panels i and j. The filling of the flux-tube with the cold plasma changes the density profile by creating a density minimum at the equator (panel n).

The plots at $\bar{t} = 700$ show that the contact between the hot and cold plasma has evolved into a pair of electrostatic shocks, one on each side of the hot ions trapped in the minimum-B field region. The shocks are indicated by arrows where flow velocities of the cold ion beams suddenly decrease (panel c). Near the shocks, the potential profile shows sharp jumps (panel k) and the density profile shows spikes (panel o).

The shocks propagate away from the "equatorially" trapped hot plasma towards the end of the flux tube, thermalizing the cold plasma just behind the shocks. The propagation of shocks can be seen by comparing the panels in columns for $\bar{t} = 700$ and 1000. The shocks propagate with a speed $V_{sh} \simeq 0.09 V_{te} \simeq C_{so}$, where $C_{so}$ is the ion-acoustic speed in the cold plasma reservoirs. As the shocks propagate away from the hot plasma, the thermalized cold plasma behind the shocks punches through the region of hot plasma where the potential barrier existed earlier. This penetration of the cold plasma is clearly seen from the $X - V_{\perp}$ plots shown in Figure 2e to 2h. As the cold ions penetrate into the minimum-B field region, where hot ions are trapped, they cool adiabaticlly as clearly seen from these plots. The penetration of cold plasma is accompanied with a reduction in the potential barrier, caused by the cold electrons being accelerated into the high potential region (panels r and s); these electrons tend to neutralize the effect of the hot ions stably trapped in the minimum-B field region.

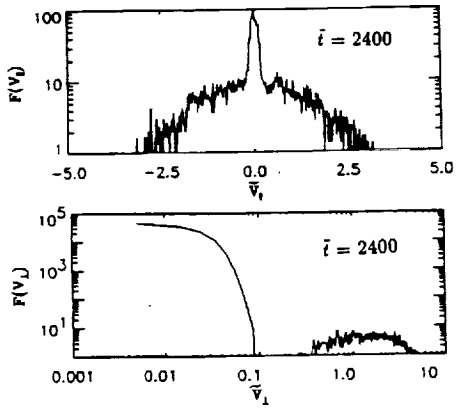


Fig. 3. Ion velocity distribution functions in the equatorial region (a) Parallel velocity distribution, (b) Perpendicular velocity distribution.

A noteworthy feature of the plasma after the spatial mixing of hot and cold plasmas is the nature of the resulting ion distribution functions in the equatorial region, as shown in Figures 3a and 3b. The parallel velocity distribution function (Figure 3a) shows a core of cold ions superimposed on a warm ion population. The perpendicular velocity distribution function (Figure 3b) also shows the cold ions, but the hot ions appear as a beam. Since the ions in the beam are nearly uniformly distributed in their phase, the beam is actually a ring in the perpendicular velocity space. The ring distribution function is the result of the trapping of the hot ions in the magnetic mirror in combination with the evolution of the electrostatic potential distribution. Some of the ions from the hot population having relatively small perpendicular velocities are lost from the mirror due to the parallel electric fields. In the absence of the electrostatic potential, one expects a

loss-cone distribution. The loss of ions with relatively low $V_\perp$, yields the ring distribution. The cold core originates from the cold ions penetrating in the minimum-B field region. The importance of these findings lies in the fact that ring types of distribution functions along with a core of cold ions can be a source of free energy for exciting equatorial waves [*Lee and Birdsall*, 1979], which can heat the latter ions. We point out that the low energy end of the ring distribution found here occurs at an energy of a few tens of eV, unlike the relatively energetic ring distribution with energy > 5 keV observed from GEOS [*Perraut et al.*, 1982].

## Conclusion and Discussion

The main conclusions of the study in this paper are the following: (1) The presence of the hot anisotropic ions trapped in the equatorial region can drastically affect the flow of the cold plasma. (2) The potential barrier associated with such a hot ion population facilitates formation of electrostatic shocks even when the cold ion beams coming from the ionosphere are highly supersonic. (3) The eventual mixing of the hot and cold plasmas produces a potentially unstable velocity distribution function for the ions. They develop a ring distribution in the perpendicular velocity. The ring distribution with $\partial f(V_\perp)/\partial V_\perp$ begins at a relatively low energy corresponding to the energy of an ion falling down the potential barrier of the order of 10 V. The ring distribution discussed here is different from the observed high energy rings (> 5 keV) produced by hot plasma injection and its subsequent convection [*Perraut et al.*, 1982].

Recent satellite observations have shown that equatorially trapped warm ions are generated by equatorial perpendicular heating of the thermal ions; the heating is caused by waves generated by an energetic hot ion population, having the temperature anisotropy $T_{i\perp}^H > T_{i\|}^H$ and/or ring type of velocity distribution [*Olsen et al.*, 1987; *Perraut et al.*, 1982 ]. *Olsen et al.* [1987] also report the reflection of cold ion beams. However, it is believed that the reflection is caused by the potential barrier set up by the thermal ions which have undergone the transverse heating. From our simulations, it appears that the hot ion population, which drives the waves by virtue of its anisotropy or ring, may reflect the fast ion beams at an earlier stage before the waves grow and consequent ion heating produces a warm anisotropic ion population.

Futhermore, before thermal ions are heated they must enter the hot plasma region. This entry is retarded by the potential barrier set up by the hot ions. Even if the hot plasma injection occurs at a stage when field-aligned flows have set up at the equator, the potential barrier is likely to expel the cold plasma from the equatorial region. The presence of thermal ions is essential in the wave generation processes. Therefore, it is suggested that the reflection of ion beams observed from DE-1 may not be necessarily caused by the equatorial perpendicular heating of thermal ions; it appears that the reflection of ion beams and heating of thermal ions are all driven by the hot ions, but heating should phenomenologically follow the reflection of upflowing ion beams.

Acknowledgments. This work was supported by NASA grant NAGW-2128 to the University of Alabama in Huntsville.

## References

Banks, P. M., A. F. Nagy, and W. I. Axford, Dynamical behavior of thermal protons in the mid-latitude ionosphere and magnetosphere, *Planet. Space Sci., 19,* 1053, 1971.

Lee, J. K. and C. K. Birdsall, Velocity space ring-plasma instability, magnetized, Part 1: Theory, *Phys. Fluids, 22,* 1306, 1979.

Olsen, R. C., C. R. Chappell, D. L. Gallagher, J. L. Green, C. R. Chappell, and R. R. Anderson, Plasma observations at the magnetic equator , *J. Geophys. Res., 92* 2385, 1987.

Perraut, S., A. Roux, P. Robert, and R. Gendrin, A systematic study of VLF wave above $F_H^+$ from GEOS-1 and -2 measurements and near relationship with proton ring distributions, *J. Geophys. Res., 87,* 6219, 1982.

Rasmussen, C. E., and R. W. Schunk, Multistream hydrodynamic modeling of interhemispheric plasma flow, *J. Geophys. Res., 93,* 14, 557, 1988.

Roux, A., S. Perraut, J. L. Ranch, C. D. Villedary , C. Kremser, A. Rorths and D. T. Young, Wave particle interactions near $\Omega He^+$ observed on board GEOS-1 and -2, 2. Generation of ion cyclotron waves and heating of $He^+$ Ions, *J. Geophys. Res., 87,* 8174, 1982.

Singh, N., Comment on "Multistream hydrodynamic modelling of interhemispheric plasma flow", by C. E. Rasmussen and R. W. Schunk, *J. Geophys., Res, 95, 17,* 272, 1990.

Singh, N. and C. B. Chan, Effects of equatorially trapped ions on refilling of the outer plasmasphere, *J. Geophys. Res., 97,* 1167, 1992.

Singh, N., R. W. Schunk and H. Thiemann, Temporal features of the refilling of a plasmaspheric flux tube, *J. Geophys. Res., 91,* 1986.

Whipple, E. C., The signature of parallel electric fields in a collisionless plasma, *J. Geophys. Res., 82,* 1525, 1977.

Wilson, G. R., J. Lin, and J. L. Horwitz, A semi-kinetic model for early stage plasmasphere refilling, 1: Effects of coulomb collisions, *J. Geophys. Res., 97,* 1189, 1992.

N. Singh, Department of Electrical and Computer Engineering, University of Alabama in Huntsville, Al 35899.

(Received November 16, 1992;
accepted January 25, 1993.)

# Comparison of Hydrodynamic and Semi-kinetic treatments for Plasma Flow Along Closed Field Lines

Nagendra Singh
Department of Electrical and Computer Engineering and CSPAR
G. R. Wilson and J. L. Horwitz
Department of Physics and CSPAR
University of Alabama in Huntsville
Huntsville, AL 35899

July 2, 1993

## ABSTRACT

Hydrodynamic and semi-kinetic treatments of plasma flow along closed geomagnetic fields lines are compared. The hydrodynamic treatment is based on a simplified 16-moment set of transport equations as the equations for the heat flows are not solved; the heat flows are treated heuristically. The semi-kinetic treatment is based on a particle code. The comparison deals with the distributions of the plasma density, flow velocity, and parallel and perpendicular temperatures as obtained from the two treatments during the various stages of the flow. In the kinetic treatment, the appropriate boundary condition is the prescription of the velocity distribution functions for the particles entering the flux tubes at the ionospheric boundaries; those particles leaving the system are determined by the processes occurring in the flux tube. The prescribed distributions are half-Maxwellian with temperature $T_0$ and density $n_0$. In the hydrodynamic model, the prescribed boundary conditions are on density ($n_0$), flow velocity ($V_0$) and temperature ($T_0$). We found that results from the hydrodynamic treatment critically depend on $V_0$; for early stages of the flow this treatment yields results in good agreement with those from the kinetic treatment, when $V_0 = \sqrt{kT_0/2\pi m}$, which is the average velocity of particles moving in a given direction for a Maxwellian distribution. During this early stage, the flows developing form the conjugate ionospheres show some distinct transitions. For the first hour or so, the flows are highly supersonic and penetrate deep into the opposite hemispheres, and both hydrodynamics and kinetic treatments yield almost similar features. It is found that during this period heatflow effects are negligibly small. When a flow penetrates deep into the opposite hemisphere, the kinetic treatment predicts reflection and setting up of counterstreaming. In contrast, the hydrodynamic treatment

yields a shock in the flow. The reasons for this difference in the two treatments is discussed, showing that in view of the relatively warm ions, the coupling of ion beams and the consequent shock formation in the offequatorial region are not likely due to the enhancements in the beam temperatures. The counterstreaming in the kinetic treatment and the shock in the hydrodynamic treatment first advance upward to the equator and then downward to the ionospheric boundary from where the flow originated. The transit time for this advancement is found to be about 1 hour for the respective models. After 2 hours or so, both models predict that the flows from the ionospheric boundaries are generally subsonic with respect to the local ion-sound speed. At late stages of the flow, when a substantial fraction of ions entering the flux tube begin to return back in the kinetic treatment, the hydrodynamic treatment with the boundary condition $V_0 = \sqrt{kT_0/2\pi m}$ yields an over-refilling, and the choice of $V_O$ becomes uncertain.

## 1. Introduction

In connection with the problem of plasmaspheric refilling, in recent years several models for plasma flow along closed magnetic field lines have been developed [*Khazanov et al.*, 1984; *Singh,et al.*, 1986; *Singh*, 1988; *Rasmussen and Schunk*, 1988; *Singh*, 1991; *Guiter and Gombosi*, 1990; *Wilson, et al.*, 1992]. These models differ in complexity in terms of describing the plasma and in including the ionosphere as a source of plasma for the refilling. In terms of describing the plasma the most contrasting feature of the existing models deals with the hydrodynamic and kinetic treatments for the flows, based on plasma fluid equations and a particle-in-cell code, respectively. For the purpose of including the ionosphere as a source of plasma for the refilling, in most studies the topside ionosphere is replaced by a set of boundary conditions on the plasma flow, except in Guiter and Gombosi [1990] who have included the generation and loss of plasma through chemical reactions in a hydrodynamic model. In this paper, we are mainly concerned with the treatments of the plasma with simple sets of boundary conditions on the plasma flow; we compare the properties of the plasma flow along closed field lines as given by hydrodynamic [*Singh*, 1992] and semi-kinetic [*Wilson et al.*, 1992] treatments.

It is generally believed that the kinetic treatment of a plasma is superior to a hydrodynamic (fluid) one. The success of a hydrodynamic treatment depends on the problem being solved and on the ingenuity of the user in chosing the hierarchy of moment equations on which fluid equations are based. In recent years, researchers in space physics have used fluid descriptions based on 13-moment [*Schunk*, 1977; *Mitchell* and *palmadesso*, 1983], and 16-moment [*Barakat and Schunk*, 1982; *Ganguli and Palmadesso*, 1987; *Gombosi and Rasmussen*, 1991; *Korosmezey et al.*, 1992, 1993] set of transport equations. In developing the moment equations, the ingenuity

lies in a series expansion of the plasma distribution function using a biMaxwellian distribution function as a base. Therefore, hydrodynamic treatment based on moment equations are good as long as the distribution function is close to a biMaxwellian. When the distribution function severely departs from a biMaxwellian and involves multistreaming of plasma particles, the moment equations are seriously handicapped, despite the sophistication incorporated through the use of higher order moment equations.

As mentioned above, recent models for plasmaspheric refilling are based on both a kinetic treatment using PIC code and hydrodynamic treatment with varying degree of sophistication in chosing the hierarchy of the moment equations. In some early models only continuity and momentum equations were solved for the ions and the electrons were assumed to remain isothermal [*Singh et al.*, 1986; *Rasmussen and Schunk*, 1988; *Singh*, 1988]. Studies which included temperature equations assumed that either the heatflow is given by the collision-dominated thermal conductively [*Khazanov et al.*, 1984; *Guiter* and *Gombosi*, 1990] or ignored the heatflow completely [*Singh*, 1992; *Singh* and *Chan*, 1992]. Neither of these assumptions correctly describe the heat transport in the refilling problem [*Singh and Horwitz*, 1992]. In the collisionless limit of plasma flow during refilling, the usual description of heatflow in terms of Spitzer thermal conductivity breaks down and such a treatment overestimates the heatflow. When the heatflow is handled by the 16-moment set of equations, the problem remains in the sense that the heatflow equations are valid for only relatively small heatflows. When the heatflow becomes large, the validity of such equations ceases and numerical instabilities result in computational work. Since, *a priory* it is not known when a large heatflow develops in a model, ad-hoc damping mechanisms are included to damp the heatflow, whether it is physically warranted

or not [*Palmadesso et al.*, 1988; Rasmussen, Private Communications]. The above problem with the 16-moment transport equations is generic; it arises irrespective of the sophistication in numerical techniques employed in solving them [*Korosmezey et al.*, 1992, 1993].

Despite the above difficulties with the hydrodynamic treatment, it has been used for practical reasons because it provides simplicity and considerable economy in computational work and depending on the plasma conditions it can work successfully. Therefore, it is advisable to keep in mind the assumptions made in using this treatment and, if possible it is even better to check the validity of this treatment by comparing its prediction against that from a kinetic treatment. Such a comparison may reveal when and how a fluid model succeeds.

The purpose of this paper is to carry out a comparison between models of the plasma flows along closed field lines based on kinetic and hydrodynamic treatments. The former treatment uses a particle-in-cell (PIC) code for ions [*Wilson et al*, 1992]. The latter one uses transport equations for the flow of mass, momentum, and parallel and perpendicular temperatures of ions [*Singh*, 1992], but the heatflow is treated heuristically [*Metzler*, 1979]. In both the treatments electrons are assumed to obey the Boltzmann law. In the present paper, the ionospheric outflows is included by imposing a set of boundary conditions on the flow of ions at an altitude of 2000 km. The choice of this altitude is primarily due to the existing models [*Wilson et al.*, 1992; *Singh*, 1992] in which ionospheric loss and generations processes for the plasma are not yet included.

The closed field lines provide the possibility of a variety of flow conditions ranging from highly supersonic to subsonic flows as an empty flux tube refills. Futhermore, the flows along closed fields lines develop counterstreaming due to interhemispheric

plasma flows. Since hydrodynamic treatments are most suspect under counterstreaming situations [*Manheimer et al.*, 1976], the comparison carried out here provides a useful guide for assessing the validity and usefulness of a hydrodynamic treatment.

We have found that for the conditions of highly supersonic flows, the two-stream hydrodynamic treatment yields flow properties in good agreement with that from the semi-kinetic treatment. Demars and Schunk[1991] reported a similar agreement based on 16-moment set of equations including heat flows. We find that the bulk parameters such as the density, flow velocity and temperatures are in good agreement even for the simpler hydrodynamic model when heatflow is included heuristically; the reason being simply that when the flow is highly supersonic, the dominant transport of heat is through the bulk flow velocity and the transport due to the thermal effects is negligibly small.

When reflection of flows causes counterstreaming, the hydrodynamic treatment gives rise to shock formation, which is not seen from the kinetic treatment. However, when the counterstreaming flows become subsonic, the hydrodynamic and semi-kinetic treatment again produce flow properties in reasonable agreement.

In order to study plasma flow in space, the plasma treatment must be supplemented by a set of boundary conditions on the flow equation. For the closed field lines, the boundary conditions are determined by the top-side ionosphere. The boundary conditions along with the demand for plasma at high altitudes produce the flow. The ionospheric boundary conditions involves generation and loss of ionospheric plasma particle species. Since here our primary goal is in identifying the kinetic and fluid-like behaviors of plasma flow and not the supply of plasma from the ionosphere and the refilling rate, we have simulated the outflow of ionospheric plasma by imposing a set of boundary conditions at an altitude of 2000 km in both the hemispheres. In the

semi-kinetic model, the imposed boundary condition is on the velocity distribution function of the ions entering the flux tube. It is assumed to be half-Maxwellian. The returning particles are self-consistently determined. In the hydrodynamic model the boundary conditions are the moments of such a distribution. Since the kinetic effect dealing with the returning particles are lost in the hydrodynamic model, the hydrodynamic model does not agree with the kinetic model when returning ion flux becomes sufficiently large. Can this disagreement be resolved by a more sophisticated treatment of the heatflow by using a complete set of 16-moment equations? In order to answer this question, further comparative studies are suggested.

The rest of the paper is organized as follows. The theoretical models are described in section 2. The comparison between the results from the two models is carried out in section 3. The main conclusions of the paper and their discussion are given in section 4.

2. Theoretical models:

The semi-kinetic model, which is based on a particle-in-cell code, has been previously described for both open [*Wilson, et al.*, 1990] and closed [*Wilson, et al.*, 1992] flux tubes. Coulomb collisions are included in the model, the collisions are implemented by pairing simulation ions according to an algorithm which conserves energy and momentum [*Takizuka and Abe*, 1977]. The algorithm yields good approximation for the collisions when the collisional relaxation time is shorter than the time step in advancing the ion motion. In the hydrodynamic model, we solve the plasma transport equations based on 16-moment approximation [e.g., see *Ganguli and Palmadesso*, 1987, and *Barakat and Schunk*, 1982]

$$\frac{\partial n}{\partial t} + \frac{\partial}{\partial s}(nV) = -nV\frac{1}{A}\frac{\partial A}{\partial s} \tag{1}$$

$$\frac{\partial V}{\partial t} + \frac{\partial}{\partial s}\left[\frac{1}{2}VV\right] = \frac{e}{m}E - (k/m)\frac{\partial T_{||}}{\partial s} - (k/m)T_{||}\frac{1}{n}\frac{\partial n}{\partial s} - g_{||}(r) - (k/m)(T_{||} - T_{\perp})\frac{1}{A}\frac{\partial A}{\partial s} + \left[\frac{\partial V}{\partial t}\right]_c \tag{2}$$

$$\frac{\partial T_{||}}{\partial t} + \frac{\partial}{\partial s}(VT_{||}) = -T_{||}\frac{\partial V}{\partial s} - \frac{1}{n}\frac{1}{A}\frac{\partial}{\partial s}(q_{||}A) + \frac{2}{n}q_{\perp}\frac{1}{A}\frac{\partial A}{\partial s} + \left[\frac{\partial T_{||}}{\partial t}\right]_c \tag{3}$$

$$\frac{\partial T_{\perp}}{\partial t} + \frac{\partial}{\partial s}(VT_{\perp}) = T_{\perp}\frac{\partial V}{\partial s} - T_{\perp}V\frac{1}{A}\frac{\partial A}{\partial s} + \frac{1}{n}q_{\perp}\frac{1}{A}\frac{\partial A}{\partial s} - \frac{1}{n}\frac{1}{A}\frac{\partial}{\partial s}(q_{\perp}A) + \left[\frac{\partial T_{\perp}}{\partial t}\right]_c \tag{4}$$

where $t$ is time; $r$ is the geocentric distance along the flux tube; $s$ is the distance along the tube from the northern ionospheric boundary at $\lambda = +\lambda_0$ (see Figure 1); n, V, $T_{||}$ and $T_{\perp}$ are the number density, flow velocity and parallel and perpendicular temperatures of ions in the plasma flow, respectively;

$q_{||}$ and $q_{\perp}$ are the heat fluxes along the magnetic field line associated with $T_{||}$ and $T_{\perp}$, respectively; E is the parallel electric field; $g_{||}$ is the component of the gravitational force parallel to the magnetic field, and $m$ and $e$ are the ion mass and charge, respectively. The collision terms denoted by $[\cdot]_c$ are calculated using Burger's Formulae [Burger, 1969], which are modified to include flow velocity corrections [*Mitchell and Palmadesso et al.*, 1983; *Ganguli and Palmadesso*, 1987] and the correction for temperature anisotropy [*Ichimaru et al.*, 1973; *Singh*, 1991].

We do not solve the heat flow equations, which have proven to be quite troublesome to solve numerically [*Palmadesso, et al.*, 1988]. The difficulty arise for a relatively large heatflow, for which the moment equations themselves become invalid. Since it is unpredictable in a model when the heatflow may be large, ad-hoc procedures are employed to attenuate the heatflow for the numerical stability of the models. This has been found to be true irrespective of the numerical techniques for solving the equations [*Palmadesso et al.*, 1988; *Koromezey et al.*, 1992, 1993; Rasmussen, private communication].

In this paper instead we have included the effects of heat flow heuristically by closely following the treatments in solar wind studies [*e.g. Metzler, et al.*, 1979]. In a collisionless plasma the usual picture of heat flow, given by $q_a = -K_a \nabla T_a$ with $K_a$ as the thermal conductivity, may not be valid because L, the mean free path, is $\gg L_T = (T^{-1}\partial T/\partial s)^{-1}$, the scale length in the temperature variation. In such a collisionless situation, the heat flux can be calculated on physical ground as follows. The heat fluxes $q_{||}^u$ and $q_{\perp}^u$ across a surface in a single direction in a plasma described by a biMaxwellian distribution function with parallel and perpendicular temperatures $T_{||}$ and $T_{\perp}$, respectively, say along the magnetic field vector, are given by

$$q_{||}^u = nkT_{||}(kT_{||}/2\pi m)^{1/2} \tag{5}$$

$$q_{\perp}^{u} = nkT_{\perp}(kT_{\parallel}/2\pi m)^{1/2} \tag{6}$$

In a uniform plasma for which the distribution function is independent of the parallel coordinates, the heatflow at any point is zero because heat flux in a given direction is cancelled by the heat flux in the opposite direction. In the presence of a spatial inhomogeniety, the cancellation is not complete, and the heat fluxes $q_{\parallel}$ and $q_{\perp}$ appearing in equations (3) and (4) can be heuristically written as [*Metzler, et al.*, 1979].

$$q_{\alpha} = \epsilon\eta nkT_{\alpha}V_{t\parallel}, \tag{7}$$

where the subscript $\alpha$ stands for $\perp$ or $\parallel$, $\epsilon = -1$ if $\partial T_{\alpha}/\partial s > 0$ and $\epsilon = 1$ if $\partial T_{\alpha}/\partial s < 0$. Thus, in the heat flow model adopted here only the sign of the heat flux depends on the temperature gradient and not its magnitude. The factor $\eta$ determines the reduction in the heat flow below the unidirectional fluxes in (5) and (6). Later on in this paper we show that $\eta$ in the range say 0.1 - 0.3 yields results in a reasonable agreement with the kinetic model, in which heat fluxes appear self-consistently. A similar model for heatflow was used by Singh[1992] for plasma flow along open field lines. In both the hydrodynamic and kinetic models adopted here, electric field E is calculated by assuming that the electrons obey the Boltzmann law and the condition of quasi-neutrality prevails.

The plasma flow along a closed field line is studied by solving an initial-boundary value problem. In the hydrodynamic model, the plasma flows originating from the conjugate ionospheres are treated as separate fluids; this treatment is termed as a two-stream model [*Singh*, 1988; *Rasmussen and Schunk*, 1988; *Singh*, 1990]. In both the models, it is assumed that at the initial time ($t = 0$) the flux tube is highly depleted. The depletion is given by $n_i = n_0(\sin\lambda/\sin\lambda_0)^6$, with the minimum density limited to $10^{-4}n_0$, where $n_0$ is the density at the ionospheric

base $\lambda = \pm\lambda_0$ (Figure 1). Initial flow velocity $V(\lambda, t = 0) = 0$ and temperatures $T_\perp(\lambda, t = 0) = T_{||}(\lambda, t = 0) = T_0 = 0.3$ eV. In the hydrodynamic model, the boundary condition for the fluids originating from the northern hemisphere are: $n_n(\lambda = \lambda_0, t) = n_0$, $V_n(\lambda = \lambda_0, t) = V_0$, $T_{||n}(\lambda_0, t) = T_\perp(\lambda_0, t) = T_0$; at the boundary $\lambda = -\lambda_0$ floating boundary condition are applied. A set of similar boundary conditions are used for the fluid originating from the southern hemisphere, but with the roles of $\lambda = \pm\lambda_0$ interchanged. In the kinetic model, the boundary conditions on ion distribution function $f(\lambda, V)$ are that $f(\lambda = \lambda_0, V \geq 0)$ and $f(\lambda = -\lambda_0, V \leq 0)$ are half-maxwellians, with a temperature $T_0$. These boundary conditions prescribe only the ions entering the flux tubes. The ions leaving the flux tubes are determined by the processes occurring inside it. A half-Maxwellian, and not a displaced Maxwellian, is chosen because of the following reasons. There is no clear observational evidence of supersonic flows along closed field lines at an altitude of 2000 km. Futhermore, our calculations show that in about 2 hours the flow in the flux tube becomes subsonic nearly all along the flux tube; only for an initial stage of about 2 hours, supersonic flows are seen. In view of such uncertainties on the the flow velocity at 2000 km, a half-Maxwellian serves the purpose of the comparative study.

## 3. Numerical Results

We compare here the properties of the flow in a flux tube with $L = 4$ as seen from the semi-kinetic and hydrodynamic models. Since the boundary value of the flow velocity ($V_0$) and the heat flow factor $\eta$ in the hydrodynamic model are free parameters, comparison is performed by varying them over physically reasonable ranges. The comparison also deals with the accumulation of plasma in the flux tube and the equatorial plasma density.

### 3.1 Initial Supersonic Flow

We recall that the hydrodynamic model is based on two-stream flow in which flows originating form the two hemispheres are treated as separate fluids, and the temporal evolution of the two streams is separately studied. Likewise, even in the semi-kinetic model, the separate identity of the ions originating from the two hemispheres is maintained. Figure 2 shows the evolution of the flow originating from the northern hemisphere as seen from the semi-kinetic model. This figure gives the phase-space density plots in $\lambda - V_{||}$ plane, where $\lambda$ is the geomagnetic latitude and $V_{||}$ is the flow velocity along the magnetic field line. The positive and negative values of $\lambda$ correspond to the northern and southern hemispheres, respectively. The darkest region in the grey-scale plots represents the highest density as indicated by the scale on the right-hand side. At time $t = .003$ *hour*, the plasma in the tube is essentially the initial plasma with a density profile given by $n = n_0[\sin\lambda/\sin\lambda_0]^6$. At later times this plasma expands into the flux tube and it is seen to cross the equator at $t = 0.25$ *hour*. Along with the expansion, new plasma enters the flux tube at the boundary $\lambda = +\lambda_0$. It is seen that by the time $t = 0.75$ *hour*, the flow has penetrated all the way to the opposite boundary at $\lambda = -\lambda_0$. It is found that the plasma reaching this boundary

is not totally lost, but it is partially reflected back, setting up a counterstreaming flow as seen from the plots for $t \geq 1$ hour. The reflected flow is seen to reach the boundary at $\lambda = \lambda_0$ by the time $t = 2$ hours. The plasma flow originating from the southern hemisphere shows a similar behavior as shown in figure 2, with the role of boundaries at $\lambda = \pm \lambda_0$ interchanged. It is worth pointing out that after reflections, ions merge with the ion stream moving in the opposite direction and they do not appear as a separate ion beam.

The possible consequences of the counterstreaming flow will be discussed later on. We now compare the above features of the flow seen from the kinetic model with those seen from the hydrodynamic model. Figures 3a to 3d show the comparison for $t = 0.5$ *hour*; these figures show the distributions of (a) density,(b) flow velocity, (c) parallel temperature, and (d) perpendicular temperature. In each panel the curve from the kinetic model is labeled, and the curves from the hydrodynamic model for three values of the heatflow reduction factor $\eta = 0$, $\eta = 0.05$ and $\eta = 0.3$ are indicated by the legend. It is seen from these figures that for most of the flux tube all four curves are quite close together, irrespective of the heatflow factor $\eta$. However, near the opposite boundary ($\lambda = -\lambda_0$), the curves from the hydrodynamic model tend to diverge from the kinetic model, depending on the value of $\eta$. This difference between the two models is attributable to the fact when the flow begins to slow down due to a relative increase in the plasma density, the hydrodynamic model predicts an increase in the parallel temperature as clearly seen for $\lambda < -36^\circ$ in Figure 3c. The increase in $T_{||}$ enhances the pressure and further slows the flow and enhances the density. In the semi-kinetic model, the temperature enhancement does not occur. Instead, a counterstreaming develops. This contrast between the two models becomes much clearer at later times, for example, at $t = 1$ *hour* for which the comparison is

shown in Figures 4a to 4d.

Figure 2 shows that at $t = 1$ *hour* the reflected ions set up counterstreaming throughout the southern hemisphere ($\lambda < 0$). Since the hydrodynamic model cannot handle the counterstreaming, the reflection process creates a shock, which is clearly seen in the density, velocity and temperature plots in Figures 4a to 4c, respectively; across the shock indicated by the arrows, density suddenly increases, flow velocity decreases and the parallel temperature also increases. We note that the hydrodynamic curves for different values of $\eta$ begin to show some difference among themselves, with the curve for $\eta = 0.3$ being closest to that from the kinetic model. It is worth pointing out that the flow velocity in the kinetic model is the average over the counterstreaming ions. The average velocity is lower than that from the hydrodynamic model over the region of the counterstreaming, but where the counterstreaming has not yet occurred ($\lambda > 30°$) the flow velocity from the two models are generally in good agreement.

The shock first propagates upward to the equator and then downward and reaches the ionospheric boundary at $\lambda = \lambda_0$ at $t \simeq 2$ hours. The propagation of the shock in the density profile is shown by the arrows in Figure 5. The transit time of about 2 hours for the shock is in agreement with the development of the counterstreaming starting in the southern hemisphere and spreading to the northern ionospheric boundary by $t = 2$ hours. (see Figure 2). We find that the heatflow plays only a minor role in the motion of the shock; the shock speed is slightly enhanced with increased heatflow $\eta$; for $\eta = 0.3$ and 0.05 the shock is already absorbed near the boundary $\lambda \simeq \lambda_0$ , while for $\eta = 0$, the shock can be still seen in the flux tube at $t = 2$ *hours*.

After the shock reaches the boundary at $\lambda = \lambda_0$, the flow in the flux tube becomes

generally subsonic with respect to the ion- acoustic speed, which is about 10 km/s with electron and ion temperatures $T_0 = 0.3ev$ at $\lambda = \pm\lambda_0$. We will discuss the subsonic stage after we examine the reason why a shock did not form during the early stage ( $\sim$ *1* hour) of the counterstreaming (Fig. 2) in the semi-kinetic model.

### 3.2 Electrostatic shock

We have just seen that a shock automatically forms in the hydrodynamic model as soon as the flow begins to reflect near the opposite boundary. On the other hand, the kinetic model does not show the shock formation. Instead, a counterstreaming flow develops. We examine this issue in terms of the conditions for shock formation and ion velocity distribution function.

According to the original suggestion of *Banks et al.*[1971], a shock should form when supersonic flow from the conjugate hemispheres collide at the equator. The flows collide as early as $t = 0.25$ *hour* ; the flows from the northern hemisphere can be seen from Figure 2 and the corresponding flow from the southern hemisphere is the mirror image of this flow with respect to the equator. When the flow begins to overlap, the shock should form through the ion-ion instability. The conditions for such an instability in a colliding situation are given by

$$1.3v_{ti} \leq V_b \leq MC_s \quad and \quad T_e > 3T_{||} \tag{8}$$

where $V_{ti}$ is the ion thermal velocity, $V_b$ is the ion beam velocity, $C_s$ is the ion-acoustic speed and $M$ is the mach number, which could be as large as 4 [*Forslund and Shonk*, 1970; *Montgomery and Joyce*, 1969]. However, it must be mentioned here that high critical Mach number $M \simeq 4$ is determined by the non-linear evolution of the electron dynamics including trapping and heating of electrons [e.g., see *Singh*, 1988]. For isothermal electrons, as it is assumed in the semi-kinetic model, $M = 1.6$

[*Tidman and Krall*, 1971]. It is worth pointing out that for large beam velocities, oblique ion waves propagating at an angle from the magnetic field are likely to be excited. However, the role of such highly oblique waves, which are likely to occur for highly supersonic beams, in momentum exchange between interpenetrating beams and shock formation is not well understood.

We examine here the likelihood of the instability occurring from the flow parameters given by the semikinetic model. First we do this exercise for $t = 30$ *minutes* when the flow has crossed the equator. Figure 6 shows the average flow velocity $V_b$, the temperature ratio $T_{\|}/T_e$ and the ion-acoustic speed $C_s$ as function of geomagnetic latitude for the flow at $t = 30$ *minutes*, shown in Figure 2. Note that the temperature ratio is plotted after multiplying it by 10, so that all the plots in Figure 6 can utilize the same vertical scale. $C_s$ is calculated from $C_s = [k(T_e + 3T_{\|})/m]^{1/2}$. The critical temperature ratio, $T_{\|}/T_e = 0.33$, for the instability is shown by the segment of the thick horizontal line in Figure 6. It is seen that the ions have sufficiently cooled down to meet instability condition on the ion temperature over an extended equatorial region ($|\lambda| \leq 20^0$). The flow coming from the opposite hemisphere shows a similar feature. The ion- acoustic speed in the equatorial region is about 8 km/s. It is seen that over the latitudinal region $|\lambda| < 20^0$, the ion beam velocity is about $V_b \simeq 2C_s$. In the semikinetic and hydrodynamic models discussed here the electrons are assumed to obey the Boltzmann law. Therefore, ion beams with such velocities are too fast to excite the ion-ion instability and thereby to form shocks in the model. Futhermore, it is important to point out that the processes which lead to shock formation, including the ion-ion instability, are microprocesses, which are suppressed in the large-scale models [*Singh and Chan*, 1993]. If electrons dynamics were rigorously included in the model and the associated microprocesses properly resolved, it is likely

that the ion-ion interaction would have occurred forming shocks.

Figure 7 shows the drift velocity $V_b$, $C_S$ and $T_{||}/T_e$ at $t = 1$ *hour* for the flow originating from the northern hemisphere. It is seen that as the ion beam penetrates into the opposite hemisphere ($\lambda < 0$), it gets progressively warmer and the temperature condition $T_{||}/T_e \leq 0.3$ is not met beyond $|\lambda| = 10^0$. Thus ion instability and shock formation are not expected. This indicates that the shock formation in the hydrodynamic model (Figures 4 and 5) is an artifact of the model.

In view of the above discussion in connection with Figures 6 and 7, it emerges that on the basis of temperature condition alone, it can be argued that if shocks form, they should be during the early stage when the ion beams begin to interpenetrate in the equatorial region. During later stages, when the beams penetrate into the opposite hemispheres the shock formation is not likely unless some how electrons are heated enhancing the temperature ratio $T_e/T_{||}$. However, as mentioned earlier the shock formation in the equatorial region requires a rigorous treatment of electron dynamics. In view of the simplified treatment of electrons in the models described here, and relatively coarse spatial and temporal resolutions afforded by them the issue of equatorial shock formation can not be settled in this paper.

### 3.3 Subsonic flow

After the initial stage of supersonic flows from the conjugate ionospheres, the flows become generally subsonic. This is predicted from both the models . Figure 8 shows the status of the flow at $t = 4$ hours, from both the hydrodynamic and semi-kinetic models. As before, there are three curves from the hydrodynamic model which are compared against the curve from the semi-kinetic model. Figure 8b shows that the flow velocities obtained for different values of $\eta$ from the hydrodynamic

model agree with the flow velocity given by the kinetic model. The maximum flow velocity of about 5 km/s seen near the boundary $\lambda = \lambda_0$ is subsonic with respect to the ion-acoustic speed $C_s = 10$ km/s. We note that the average flow velocity peaks slightly above the boundary in both hydrodynamic and kinetic models. The peaking is a consequence of the boundary conditions at $\lambda = \lambda_0$ and the acceleration of ions by the pressure and electric field distributions in the close vicinity of the northern boundary of the flux tube.

Figures 8a, 8c, and 8d show that for the subsonic flow the density and temperature structures critically depend on the heatflow factor $\eta$. For $\eta = 0.3$, the hydrodynamic model yields results in good agreement with those from the kinetic model. When $\eta$ becomes too small ($\eta \leq 0.05$), the structures in the density and temperature profiles markedly differ from the kinetic model; the density structure shows an extended density cavity in the equatorial region, where parallel temperature is relatively high [*Singh*, 1991]. Futhermore, for low values of $\eta$ there is density enhancement and correspondingly a low parallel temperature in the southern hemisphere. When heatflow factor is sufficiently large ($\eta > 0.15$), such structures in $n(\lambda)$ and $T_{\|}(\lambda)$ are washed away. In a recent paper, Ho et al [ 1993] computed the parameter $\eta$ from the semikinetic model for flows along open flux tubes and it was found to be $> 0.1$.

The comparison between the hydrodynamic and kinetic results at $t = 12$ *hours* is shown in Figures 9a to 9d. The density and temperature structures at this stage are qualitatively similar to that at $t = 4$ *hours* as shown in Figures 8a to 8d. However it is seen that at $t = 12$ *hours*, the density and temperature profiles even for $\eta = 0.05$ have begun to compare well with that for $\eta = 0.3$, for which the density distribution agrees well with that given by the semikinetic treatment. The discrepancy between the densities predicted by the kinetic treatment and the hydrodynamic one for $\eta =$

0.3 is bounded by 15 %, for most part of the flux tube, except near the southern boundary $\lambda = -\lambda_0$.

The runs for the comparison between the hydrodynamic and kinetic models were carried on until $t = 18$ *hours*. For time $t > 12$ hours, it was found that the hydrodynamic model systematically yields densities higher than that given by the semi-kinetic model. Figure 10 shows the comparison between the equatorial densities as obtained from the two models . This figure shows the temporal evolution of the equatorial densities found from the kinetic (solid line) and the hydrodynamic (broken line curves) models. For the latter model, the densities are plotted for different values of the flow velocity ( $V_0$) at the boundaries $\lambda = \pm\lambda_0$. We remind ourselves that the results from the hydrodynamic model shown in Figures 3, 4, 5, and 8 are for a flow velocity $V_0 = (kT_0/2\pi m)^{1/2} = 0.39V_t$. We notice from Figure 10 that for this boundary value of the flow velocity, the kinetic and hydrodynamic curves are remarkably close for $t \leq 12$ hours. This implies that this boundary value of the flow velocity closely corresponds to the input flux determined by a half-Maxwellian distribution function, which is imposed as boundary condition in the kinetic model. For $t > 12$ hours, the boundary value of $V_0 = 0.39V_t$ yields an over-refilling compared to the kinetic model. This simply implies that the net influx of ion into the flux tube at the ionospheric boundaries steadily decreases in the kinetic model, primarily due to the ions flowing out of the flux tube. On the other hand, in the hydrodynamic model, the influx is primarily determined by the imposed flow velocity and it remains constant. This is demonstrated by comparing the temporal evolution of the total plasma content in the flux tube as seen from the two model.

Figure 11 shows the total content as a function of time. As in Figure 10, for the hydrodynamic model the curves are for different values of the imposed velocity

at the boundary. It is seen that for $V_0 = 0.39V_t$, the hydrodynamic model yields nearly the same total plasma content as the kinetic model with nearly the same rate of increase in it for $t \leq 12$ hours. At later times, the content from the kinetic model shows a tendency toward saturation because the rate of increase in the content continuously decreases. Even in the hydrodynamic model there is a tendency towards the decreasing rate, but the decrease is much slower. This difference in the influx of the ions form the two model has a simple explanation. In the kinetic model, some of the ions have the liberty to exit the flux tube as they are scattered by Coulomb collisions, or as they simply flow out. On the other hand, in the hydrodynamic model the plasma entering the flux tube can leave the system only through the opposite boundary, where the flow velocity becomes exceedingly small after the shock phase ($t > 2$ hours). This implies that in the hydrodynamic model there is no provision for the plasma to leave the system. The slight tendency toward the saturation in the hydrodynamic model is due to the changing plasma condition near the boundary where the flow originates. As the plasma density near this boundary increases, the influx into the flux tends to decrease.

Figures 10 and 11 also show the equatorial density and the total plasma content from the hydrodynamic model for $V_0 = 0.1V_t$ and $V_0 = 0$. It is seen that even for $V_0 = 0$, the equatorial density and the total content are increasing with time and, in about 48 hours, they tend to approach the corresponding results from the kinetic model. It may sound strange how refilling can occur with a boundary condition of $V_0 = 0$! The refilling of a flux tube with zero flow velocity as boundary conditions in a hydrodynamic model was previously described by *Singh et al.*, [1986].

The ion flux developing near the boundaries from the kinetic model and the hydrodynamic model for $V_0 = 0.39V_t$ during the early times ($t < 12$ *hours*) is $1.8 \times 10^8$

ions $cm^{-2}s^{-1}$. In the kinetic model, this flux continuously decreases because some of the ions entering the flux tube eventually leave. However, in the hydrodynamic model the plasma entering the flux tube remains in it, causing the over-refilling for $t > 12$ *hours* when $V_0 = 0.39V_t$. When $V_0 = 0$, the hydrodynamic model yields a flux of $\leq 10^8$ ions $cm^{-2}s^{-1}$ and it continuously decreases as the forces (determined by density and temperature gradients) on the ions accelerating them into the flux tube from the boundary cells diminishes with the refilling. It is worth mentioning that the comparison carried out above is based on the simplified boundary conditions in the kinetic and fluid treatments and a heuristic treatment of the heatflow. A comparison of the plasma treatments without these simplifications will be worthwhile.

A comparison of plasma distributions in the flux tube at a relatively late time ($t = 48$ hours), as obtained from the two models, is shown in Figures 12a to 12d. For the hydrodynamic model, $\eta = 0.3$, and the distributions are given for three values of the boundary velocity, $V_0 = 0.39V_t$, $0.1V_t$, and $0$. Density profiles in Figure 12a show the over-refilling for $V_0 = 0.39V_t$, but when $V_0$ is reduced below $0.1V_t$, the density profiles from the two models disagree near the boundary $\lambda = \lambda_0$, but away from it the agreement considerably improves. The disagreement near the boundary is also reflected in the velocity profiles in Figure 12b. Despite the above disagreement in the density and velocity profiles near the boundary, the temperature structures obtained from the two models are nearly identical. Temperature is nearly isotropic ($T_{||} \approx T_{\perp}$); it rises to about 0.4 eV in the equatorial region from the boundary value of 0.3 eV. In the late stage of the refilling, the similarity between the temperature profiles, despite the differences in the density and velocity profiles from the two models, can be understood by examining the temperature equations (3) and (4) and the flow properties. Since the flow velocity is small, the velocity profile has little

effect on the temperature profiles. The maximum flow velocity in a localized region near the boundary is 2.5 km/s, compared to the thermal velocity of 5.5 km/s and ion-acoustic speed of 10 km/s. The density distribution affects the temperature distribution through the heatflow terms in equations (3) and (4). In the late stage of the flow when the gradients have smoothed out and the densities are relatively large, the density distribution also has insignificant effects on the heat flow.

## 4. Conclusion and Discussion

We have carried out a comparison between semi-kinetic and hydrodynamic models for plasma flow along closed magnetic field lines. The comparison has direct relevance to the problem of plasmaspheric refilling. It is found that the comparison does not depend only on the plasma physics afforded by the models, but it also strongly depends on the boundary condition on the flow velocity. In a kinetic model, an appropriate boundary condition is to prescribe the velocity distributions of the inflowing ions to be half- Maxwellian for $V \geq 0$ at $\lambda = \lambda_0$ and for $V \leq 0$ at $\lambda = -\lambda_0$. In the hydrodynamic model, this boundary condition corresponds to the drift velocity $V_0 = (kT_0/2\pi m)^{1/2}$. A comparison of results from the two models with such boundary conditions revealed the following important features of the flows.

1. When supersonic flows develops in response to a sudden depletion in a flux tube, the hydrodynamic and kinetic models yield distribution of density, flow velocity and temperatures in generally good agreement. The temperature distributions in the region of supersonic flows are found to be remarkably similar, showing small effect of the heatflow. It is worth pointing out that *Demars and Shunk* [1991] compared the behavior of a highly supersonic plasma flow from a hydrodynamic model based on a more complete (16-moment) set of equations with that from a semi-kinetic model, demonstrating a good agreement. We have demonstrated here that, for a highly supersonic flow, even a much simpler set of hydrodynamic equations are adequate. It is physically explained by the fact that the transport of heat in a supersonic flow is dominated by the large drift velocity and not by the heatflow process. Mathematically speaking,

it implies that the heatflow terms are negligibly small compared to the convective terms in the temperature equations.

2. Both models show reflection of the supersonic flow when it penetrates deep into the opposite hemisphere. Since even a two-stream hydrodynamic model can not handle the counterstreaming for a given flow, the reflection automatically leads to a shock formation [*Rasmussen and Schunk,* 1988; *Singh,* 1991]. The shock first moves upward toward the equator and then downward to the ionospheric boundary. An examination of the plasma conditions for shock formation shows that the shock seen in the hydrodynamic model is an artifact of the model; the ion beams are found to be too warm to excite the ion-ion instability which can subsequently produce a shock. The semi-kinetic model shows the development of counterstreaming for the flow; the counterstreaming advances to the equator and downward to ionospheric boundary. It turns out that the transit time of the shock all the way to the ionospheric boundary and the time for the counterstreaming to spread to this boundary are nearly the same, about 2 hours. In a previous paper, *Singh* [1991] reported the shock transit time to be about 4 hours, which is in error due to a normalization factor of 2. In view of the short transit time of the shock, the shock formation does not significantly affect the refilling as evidenced by the comparison of the flows from the hydrodynamic and kinetic models for later times.

   Lack of shock formation in the equatorial region, when the ion beams begin to interpenetrate [*Banks et al.*, 1971] is uncertain in view of the spatial and temporal resolutions afforded by a large-scale model and the simplicity in handling the electron dynamics by the Boltzmann law.

3. After about 2 hours, the flow in each hemisphere becomes subsonic with respect to the ion-acoustic speed. This is seen from both the models.

4. A comparison of the total plasma contents and the equatorial densities from the two models indicates a good agreement up to about $t \simeq 12$ hours, after which the hydrodynamic model indicates over-refilling of the flux tube. The over-refilling is traced to the inability of our hydrodynamic model to control the net plasma inflow by the returning particles. The inflow is determined by the imposed boundary conditions and the outflow of plasma is exceedingly small. On the other hand, in the kinetic model the influx gradually decrease due to ions returning from the flux tube, showing a tendency toward saturation in the refilling in about 2 days. It is worth pointing out that it will be useful to perform a study comparing the models based on the kinetic and hydrodynamic treatments by relaxing some of the simplifications in terms of boundary conditions and in handling of the heat flow in the latter treatment. The boundary conditions can be relaxed by including the ionospheric plasma generation processes at low altitudes [*Guiter and Gombosi*, 1990].

When the boundary flow velocity in the hydrodynamic model reduces below $V_0 = (kT_0/2\pi m)^{1/2}$, there is an initial underfilling, but eventually the refilling from this model catches up to that given by the semi-kinetic model. For example when $V_0 = 0$, the degree of refilling from the two models, in terms of both the equatorial density and the total plasma content in the flux tube, becomes approximately the same in about 2 days.

In some previous studies [*Singh, et al.*, 1986; *Rasmussen and Schunk*, 1988; *Singh,*

1991], a boundary condition of zero flow velocity was used. It may appear strange that a refilling occurs with this boundary condition on the flow velocity. The issue is briefly revisited here.

From the comparison of the plasma contents and the equatorial densities given by the models, it is concluded that after about 12 hours, the choice of boundary condition in the hydrodynamic model is quite uncertain . In view of this uncertainty, the choice of zero-velocity boundary could be useful during the late stage of the refilling, it yields under-refilling only near the boundaries, where the density and average flow velocity show a discontinuity in the flow. Otherwise, over the rest of the flux tube the density and flow velocity are in quite good agreement with those given by the kinetic model.

The hydrodynamic model described here is a two-stream model and includes equation for the parallel and perpendicular temperatures. Single-stream hydrodynamic models [*Singh et al.*, 1986; *Guiter and Gombosi*, 1990] suffer from the shortcoming that they generate shocks at the equator whether the plasma conditions allow them or not. The single- and two-stream models with assumed temperature isotropy suffer from the shortcoming that the shock transit time is fairly long and major part of the refilling occurs through supersonic flows from the ionospheres [*Singh et al.*, 1986, *Rasmussen and Schunk*, 1988; *Singh*, 1991]. This is in contrast to the two-stream model with a self-consistent treatment of the temperature anisotropy; this model yields evolution from supersonic to subsonic flows at the same time scale as the kinetic model. In this sense, the heuristic treatment of the heatflow described in this paper appears to be adequate. This treatment also appears to be adequate even in the subsonic stage as long as the flow velocity near the boundary is relatively large near the thermal speed, for example, for $t < 12$ hours in our present calculations.

However, when the flow velocity becomes sufficiently low so that a large fraction of injected ions in the kinetic model begin to return from the immediate vicinity of the boundary, the boundary conditions for the hydrodynamic model diverges from that of the kinetic treatment, because this model does not allow for a return flux for a given stream. Can this situation be improved by a more rigorous treatment of the heatflow and/or by properly including the ionospheric plasma supply [*Guiter and Gombosi*, 1990]? In order to answer this question, it will be useful to compare models based on (1) the heuristic heatflow treatment, (2) a more sophisticated treatment of the heatflow using 16-moment set of transport equations, and (3) the semikinetic treatment, and all models properly including the analogous ionospheric boundary conditions. If the model (1) compares well with the latter ones, the computational effort in using transport equations for modeling space plasma will be considerably reduced.

## ACKNOWLEDGMENTS

This work was supported by NASA grants NAGW-2128, NAG8-239 and NSF grant ATM 8911799 made to the University of Alabama in Huntsville.

# REFERENCES


Banks, P. M., A. F. Nagy, and W. I. Axford, Dynamical Behavior of Thermal Protons in the Mid-Latitude Ionosphere and Magnetosphere, *Planet. Space Sci., 19,* 1053, 1971.

Barakat, A. R., and R. W. Schunk, Transport Equations for Multicomponent Anisotropic Space Plasma: A Review, *Plasma Phys., 24*, 389, 1982.

Burgers, S. M., Flow Equations for Composite Gases, *Academic, Orlando, Fla.,* 1969

Demars, H. G. and R. W. Schunk, Comparison of Semikinetic and Generalized Transport Models of the Polar Wind, *J. Geophys. Res. Lett ., 18,* 1841, 1991.

Forslund D. W., and C. R. Shonk, Formation of Electrostatic Collisionless Shocks, *Phys. Rev. Lett., 25,* 1699, 1970.

Ganguli, S. B., and P. J. Palmadesso, Plasma Transport in the Auroral Current Region, *J. Geophys. Res., 92*, 8673, 1987.

Gombosi, T. and C. E. Rasmussen, Transport of gyration-dominated space plasmas of thermal origin 1. Generalized transport equations, *J. Geophys. Res., 96*, 7759, 1991.

Guiter, S. M., and T. Gombosi, The Role of High-speed Plasma Flows in Plasmaspheric Refilling, *J. Geophys. Res., 95*, 10,427, 1990.

Ho, W., J. L. Horwitz, N. Singh and G. R. Wilson, Comparison of time-dependent and hydrodynamic models for plasma expansion and density perturbation in the polar-wind, *J. Geophy. Res., in press*, 1993.

Ichimaru, S., Basic Principles of Plasma Physics, *The Benjamin, Cummings publishing company, Inc., Reading, Massachussets, Chapt. 10,* 1973.

Khazanov, G. V., M. A. Kuen, Yu. V. Konikov and I. M. Sidorov, Simulation of ionosphere-plasmasphere coupling taking into account ion inertia and temperature anisotropy, *Planet. Space Sci., 32,* 585, 1984.

Kórösmezey, *Á.*, C. E. Rasmussen, T. I. Goubosi, and G. V. Khazanov, Anisotropic ion heating and parallel $o^+$ acceleration in regions of rapid E $\times$ B convection, *Geophys., Res. Lett., 19,* 2297, 1992.

Kórösmezey, *Á.*, C. E. Rasmussen, T. I. Goubosi, and B. Van Leer, Transport of Gyration-Dominated Space Plasmas of Thermal Origin 2., Numerical Solutions, *J. Computational Physics,* in press, 1993.

Manheimer, W. M., M. Lanks, and R. W. Clark, Multistreaming and the Viability of Fluid Codes, *Phys. Fluids, 19,* 1788, 1976.

Metzler, N., S. Cuperman, M. Dryer, and P. Rosenau, A Time-Dependent Two-Fluid Model with Thermal Conduction for the Solar Wind, *Astrophys. J., 231,* 960, 1979.

Mitchell, H. G., and P. J. Palmadesso, A dynamic model for the auroral field line plasma in the presence of field-aligned current, *J. Geophys. Res, 88,* 2131, 1983.

Montgomery, D. and G. Joyce, Shock-like Solutions of Electrostatic Valsov Equation, *J. Plasma Physics, 3, part 1,* 1, 1969.

Palmadesso, P. J., S. B. Ganguli, and H. G. Mitchell, Jr., Multi-Component Fluid Simulations of Transport Processes in the Auroral Zones in *Modeling Magnetospheric*

*Plasma, Geophys. Monogr. Ser.*, vol. 44, edited by T.E.Moore and J.H. Waite, Jr., p. 133, AGU, Washington D.C., 1988.

Rasmussen, C. E., and R. W. Schunk, Multistream Hydrodynamic Modeling of Interhemispheric Plasma Flow, *J. Geophys. Res., 91,* 14557, 1988.

Schunk, R. W., Mathematical Structure of Transport Equations for Multispecies Plasma Flow, *Rev. Geophys. Space Phys., 15,* 429, 1977.

Singh, N., R. W. Schunk, and H. Thiemann, Temporal Features of the Refilling of a Plasmaspheric Flux Tube, *J. Geophys. Res.. 91,* 13433, 1986.

Singh, N., Refilling of a Plasmaspheric Flux Tube-Microscopic Plasma Processes, in *Magnetospheric Plasma, Geophys Monogr. Ser.*, vol. 44, Edited by T. E. Moore and J. H. Waite, Jr., p.87, AGU, Washington, D.C., 1988.

Singh, N., Comment on "Multistream Hydrodynamic Modeling of Interhemispheric Plasma Flow" by C. E. Rasmussen and R. W. Schunk, *J. Geophys. Res., 95,* 17273, 1990.

Singh, N., Role of Ion Temperature Anisotropy in Multistage Refilling of the Outer Plasmaspheric. *Geo. Res. Lett., 18,* 817, 1991.

Singh, N., Plasma Perturbations Created by Transverse Ion Heating Events in the Magnetosphere, *J. Geophys. Res.. 97,* 4235, 1992.

Singh, N. and C. B. Chan, Effects of equatorially trapped ions as refilling of the plasmasphere, *J. Geophys. Res., 97,* 1167, 1992.

Singh, N. and C. B. Chan, Numerical Simulation of plasma processes driven by transverse ion heating, *J. Geophys. Res., in press,* 1993.

Singh, N. and J. L. Horwitz, Plasmasphere refilling: recent observations and modeling, *J. Geophys. Res.*, *97*, 1047, 1992.

Takizuka, T. and H. Abe, A binary collision model for plasma simulation with a particle code, *J. Comp. Phys.*, *25*, 205, 1977.

Tidman, D. A., and N. A. Krall, Shock Waves in Collisionless Plasmas, *Wiley-Interscience, New York*, 1971.

Wilson, G. R.,C. W. Ho, J. L. Horwitz, N.Singh, and T.E. More, A New Kinetic Model for Time-Dependent Polar Plasma Outflow: Initial Results, *Geophys. Res. Lett.*, *17*, 263, 1990.

Wilson, G. R., J. L. Horwitz, and J. Lin, A Semi-Kinetic Model for Early Stage Plasmasphere Refilling, 1: Effects of Coulomb Collisions, *J. Geophys Res.*, *91*, 1109, 1992.

Figure Captions:

Figure 1. Geometry of a closed magnetic flux tube. The latitudinal angle $\lambda$ and the geocentric distance r are shown. The ionospheric boundaries are at $s = 0(\lambda = \lambda_0)$, and $s = s_{max}(\lambda = -\lambda_0)$

Figure 2. Temporal evolution of the flow originating from the northern hemisphere; phase-space $(s - V_{||})$ plots are shown. The plot at $t = .003$ *hour* nearly shows the initial plasma in the flux tube.

Figure 3. Comparison of flows from semi-kinetic and hydrodynamic models at $t = 30$ *minutes* For the latter model flows are given for $\eta = 0$, 0.05 and 0.3: (a) density, (b) flow velocity, (c) parallel temperature and (d) perpendicular temperature distributions. For most latitudes, the curves are so close together that it is difficult to distinguish them.

Figure 4. Same as Figure 3, but at $t = 1$ *hour* The hydrodynamic curves are distinguished by the presence of a shock which is manifested by sudden jumps in density, flow velocity and parallel temperature near $\lambda \simeq -25$. Shocks are indicated by the arrows.

Figure 5. Propagation of the shock is shown through the jump in the density profiles at (a) $t$ =1 hour, (b) $t$ = 1.5 hours and (c) $t$ = 2 hours. For the purpose of comparison the curve from the kinetic model and three curves for $\eta = 0, 0.05$, and 0.3 from the hydrodynamic model are shown. Shocks are indicated by arrows.

Figure 6. Distribution of flow parameters from the kinetic model. The average flow velocity $V_b$, ion-acoustic speed $C_s$ and the temperature ratio $T_{||}/T_e$ for ions with $V_{||} > 0$ are shown for the purpose of instability analysis at $t = 30$ *minutes*. The corresponding curves for $V_{||} < 0$ can be deduced from the symmetry considerations.

Figure 7. Same as Figure 6. but at $t = 1$ *hour.*

Figure 8. Same as Figure 4. but at $t = 4$ *hours.*

Figure 9. Same as Figure 4, but at $t = 12$ *hours.*

Figure 10. Temporal evaluation of the equatorial density from the kinetic model and from the hydrodynamic model for three values of $V_0$, $0.39\,V_t$, $0.1\,V_t$, and $0\,V_T$.

Figure 11. Temporal evolution of the total plasma content in the flux tube for the kinetic and hydrodynamic models.

Figure 12. Distribution of (a)density, (b) flow velocity, (c) parallel temperatures and (d) perpendicular temperature at $t = 48$ *hours* . All vertical scales are linear in this Figure. There are three curves from the hydrodynamic model for $V_0 = 0$, $0.1\,V_t$, and $0.39\,V_t$.

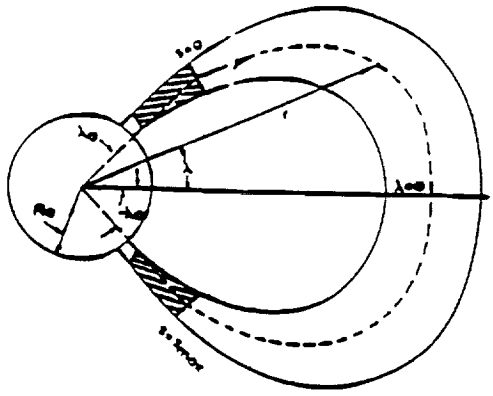

Fig. 1

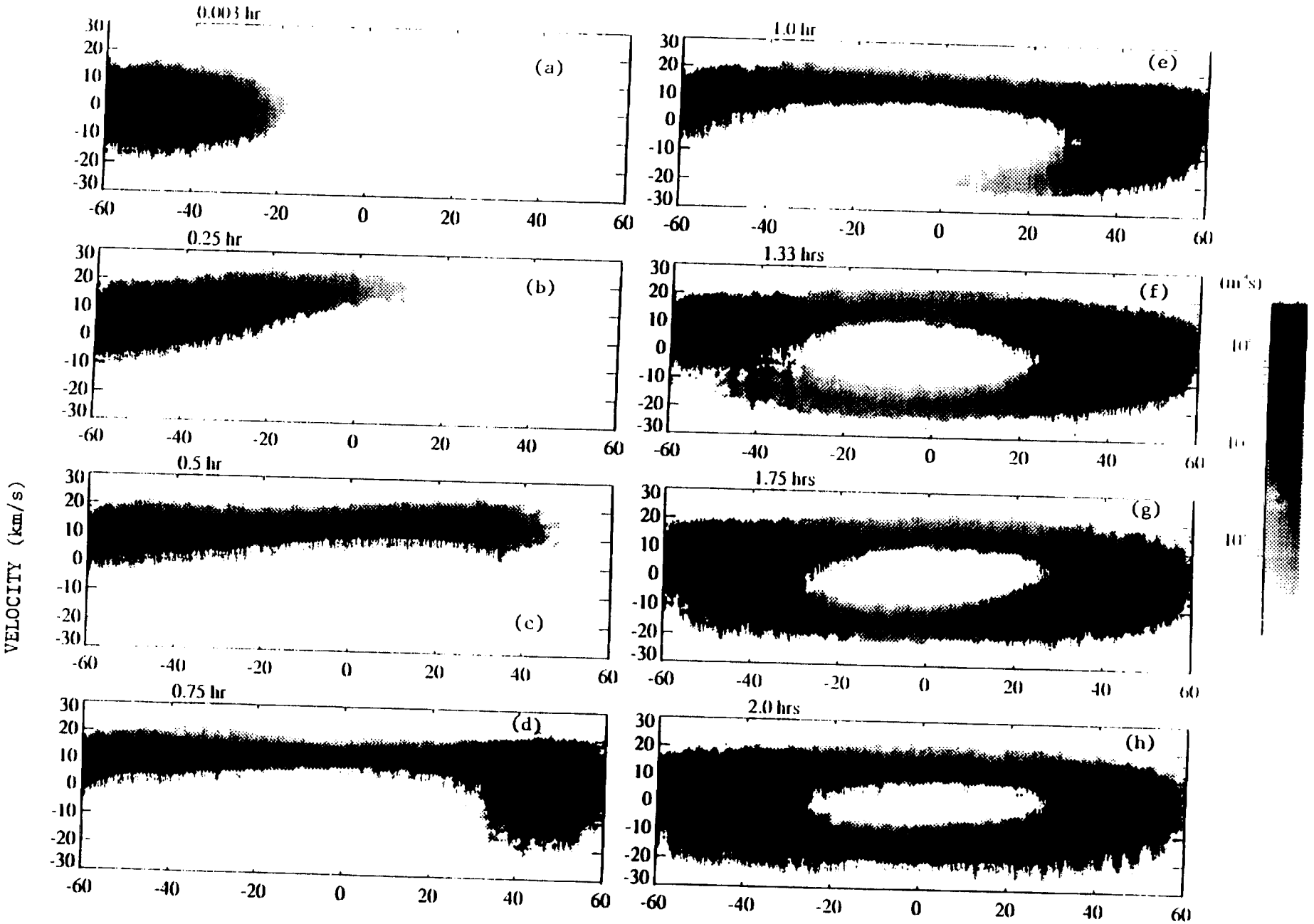
0.003 hr
(a)
1.0 hr
(e)
0.25 hr
(b)
1.33 hrs
(f)
0.5 hr
(c)
1.75 hrs
(g)
0.75 hr
(d)
2.0 hrs
(h)
VELOCITY (km/s)
GEOMAGNETIC LATITUDE (DEGREES)

Fig. 2

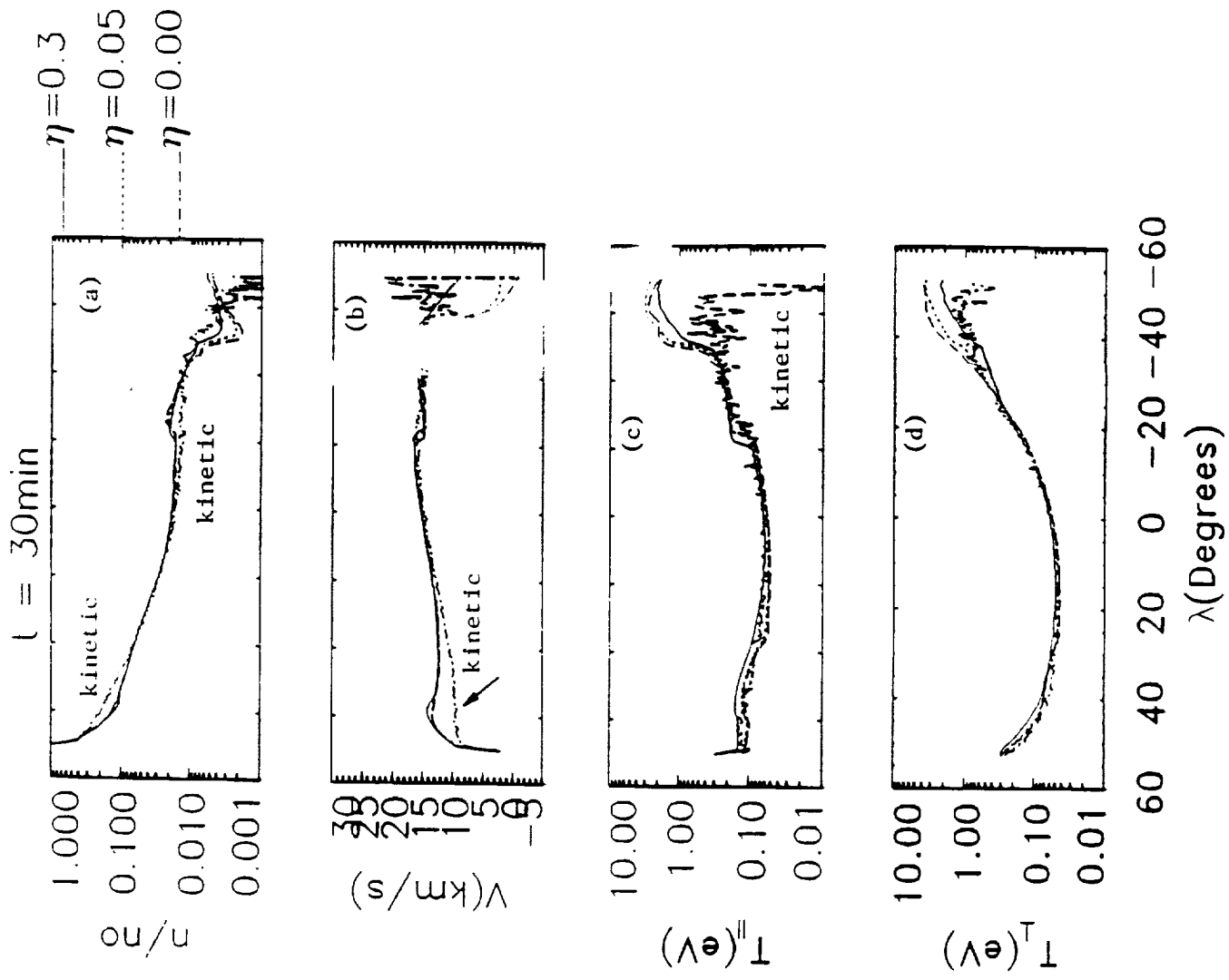
t = 30min
η=0.3
η=0.05
η=0.00
(a)
kinetic
kinetic
n/no
1.000
0.100
0.010
0.001
(b)
kinetic
V(km/s)
30
20
15
10
5
0
−5
(c)
kinetic
T∥(eV)
10.00
1.00
0.10
0.01
(d)
T⊥(eV)
10.00
1.00
0.10
0.01
60 40 20 0 −20 −40 −60
λ(Degrees)

Fig. 3

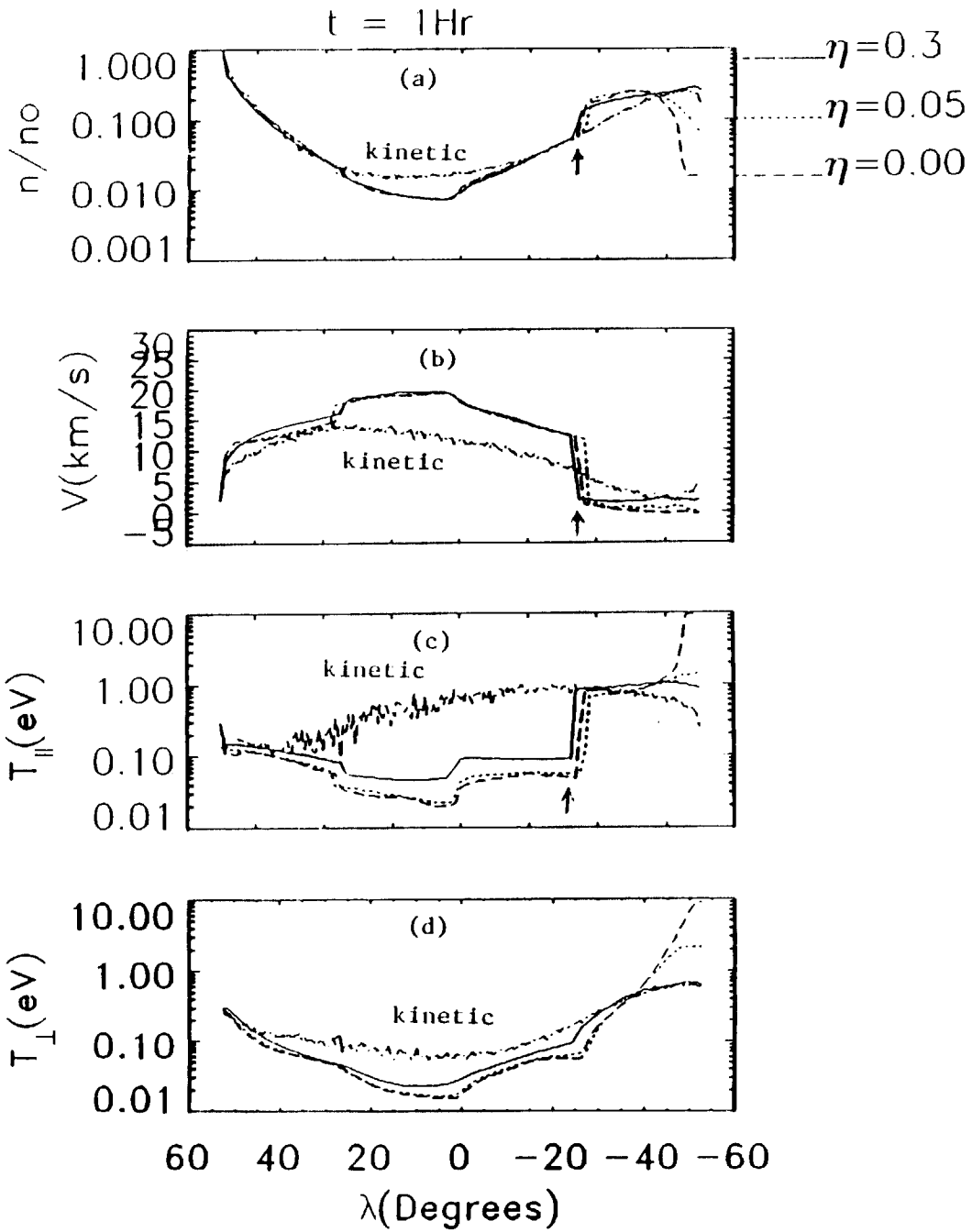
t = 1Hr
(a)
kinetic
n/no
1.000
0.100
0.010
0.001
η=0.3
η=0.05
η=0.00
(b)
kinetic
V(km/s)
30
25
20
15
10
5
0
−5
(c)
kinetic
T∥(eV)
10.00
1.00
0.10
0.01
(d)
kinetic
T⊥(eV)
10.00
1.00
0.10
0.01
60 40 20 0 −20 −40 −60
λ(Degrees)

Fig. 4

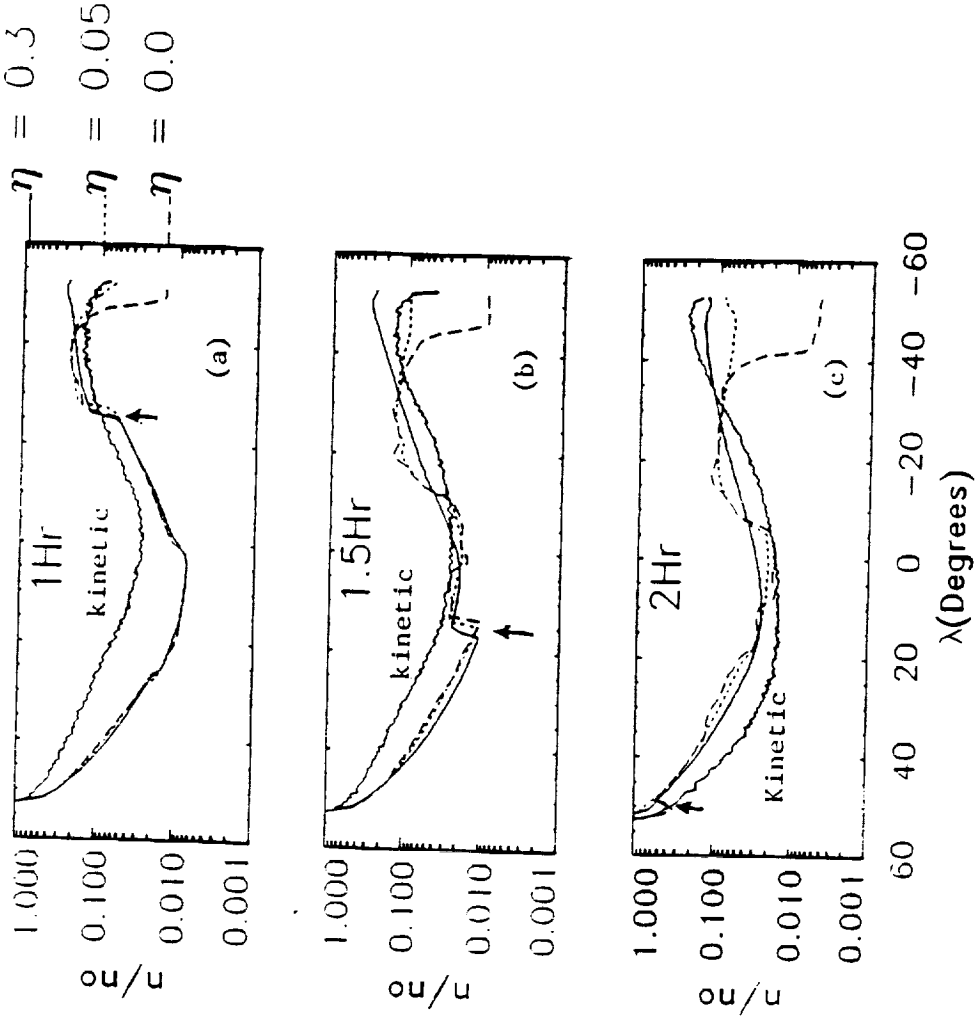
η = 0.3
η = 0.05
η = 0.0
1Hr
kinetic
(a)
1.5Hr
kinetic
(b)
2Hr
Kinetic
(c)
n/no
1.000
0.100
0.010
0.001
60
40
20
0
-20
-40
-60
λ(Degrees)

Fig. 5

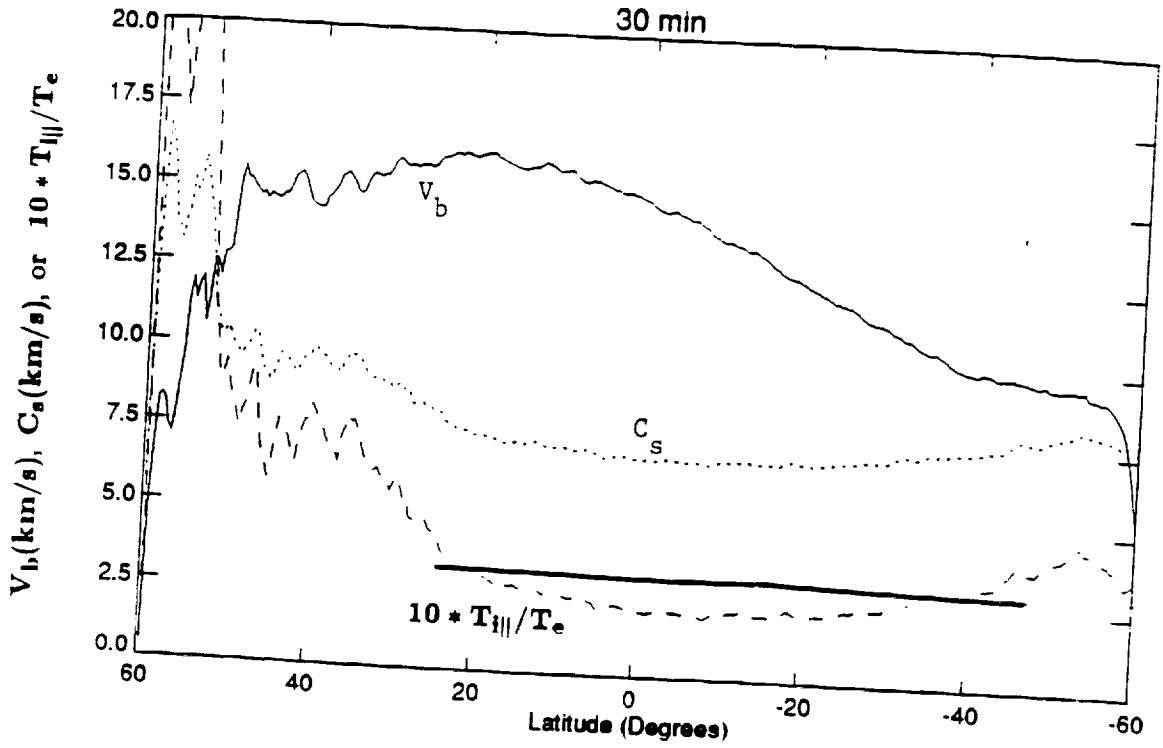
30 min
20.0
17.5
15.0
12.5
10.0
7.5
5.0
2.5
0.0
$V_b$
$C_s$
$10 * T_{i||}/T_e$
60
40
20
0
-20
-40
-60
Latitude (Degrees)
$V_b$(km/s), $C_s$(km/s), or $10 * T_{i||}/T_e$

Fig. 6

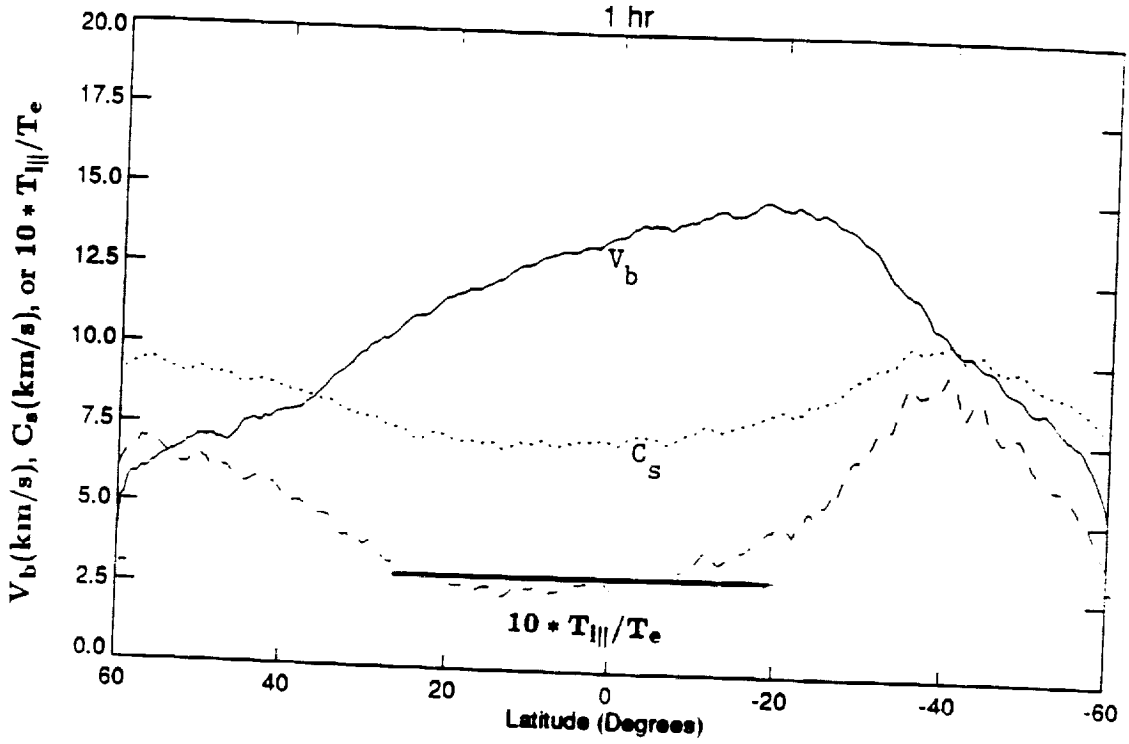
1 hr
20.0
17.5
15.0
12.5
10.0
7.5
5.0
2.5
0.0
$V_b$(km/s), $C_s$(km/s), or 10 * $T_{|||}/T_e$
$V_b$
$C_s$
10 * $T_{|||}/T_e$
60
40
20
0
-20
-40
-60
Latitude (Degrees)

Fig. 7

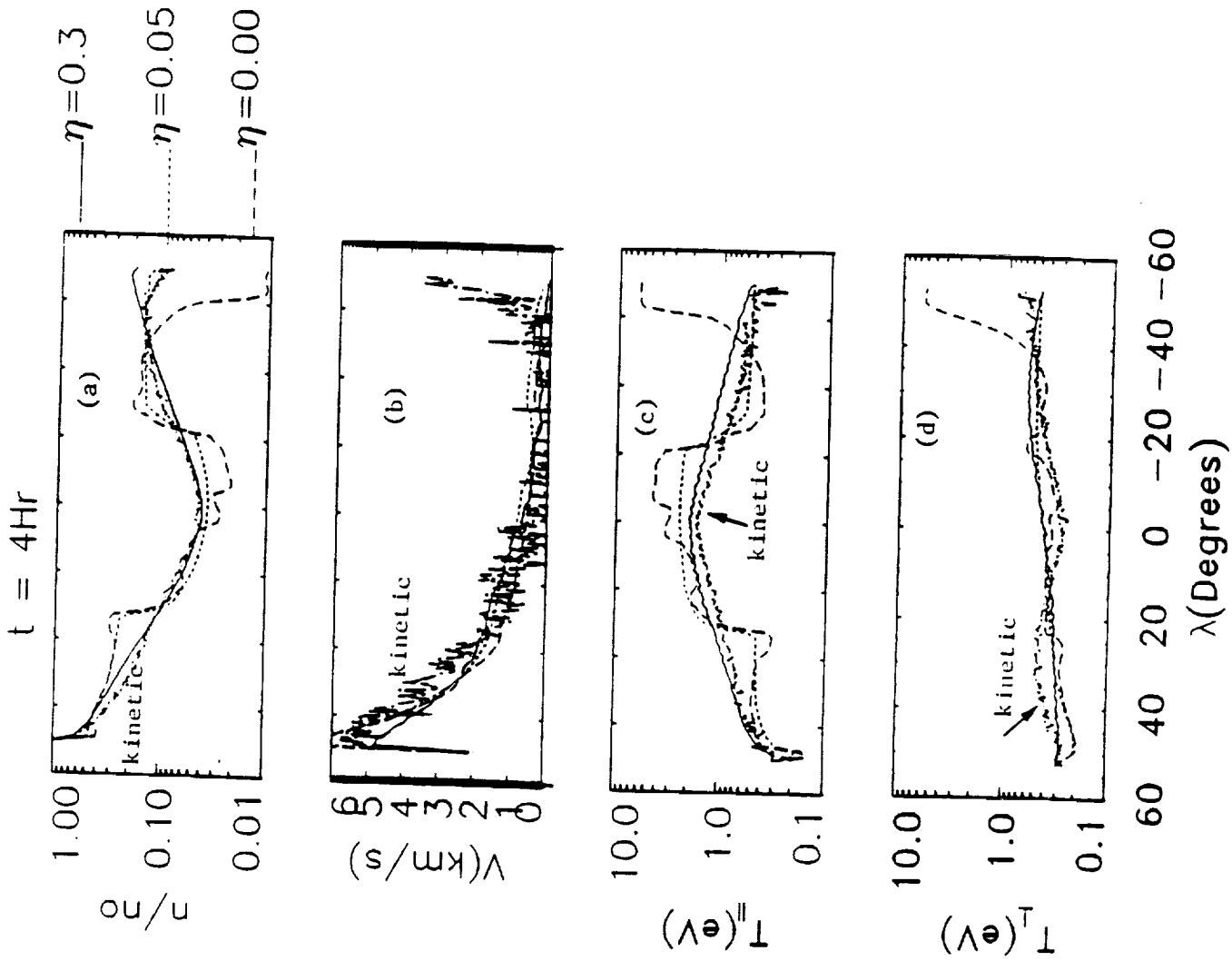
t = 4Hr
η=0.3
η=0.05
η=0.00
(a)
kinetic
n/no
1.00
0.10
0.01
(b)
kinetic
V(km/s)
6
4
3
2
1
0
(c)
kinetic
T∥(eV)
10.0
1.0
0.1
(d)
kinetic
T⊥(eV)
10.0
1.0
0.1
60 40 20 0 −20 −40 −60
λ(Degrees)

Fig. 8

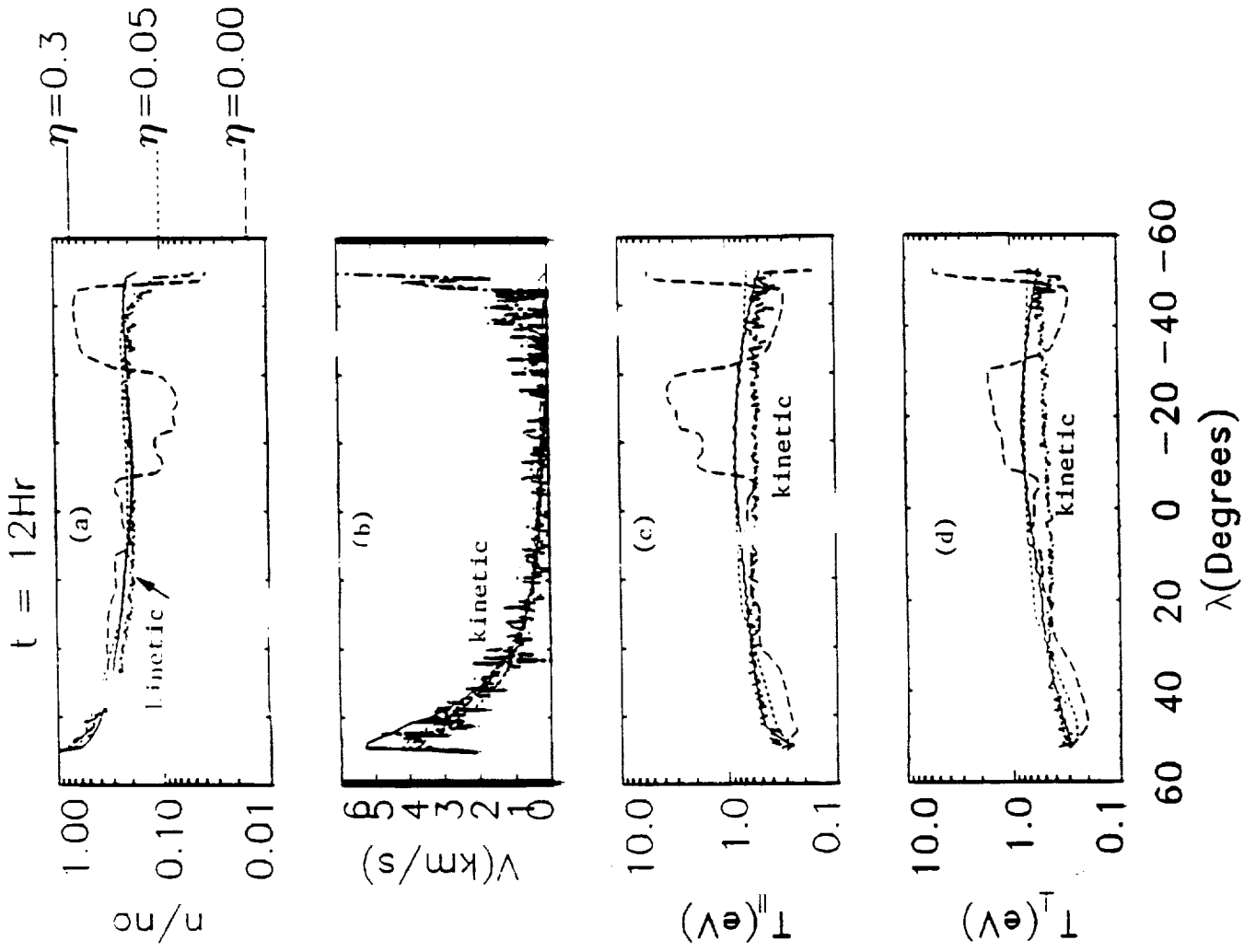
t = 12Hr
η=0.3
η=0.05
η=0.00
(a)
kinetic
n/no
1.00
0.10
0.01
(b)
kinetic
V(km/s)
6
4
3
2
1
0
(c)
kinetic
T∥(eV)
10.0
1.0
0.1
(d)
kinetic
T⊥(eV)
10.0
1.0
0.1
60 40 20 0 −20 −40 −60
λ(Degrees)

Fig.9

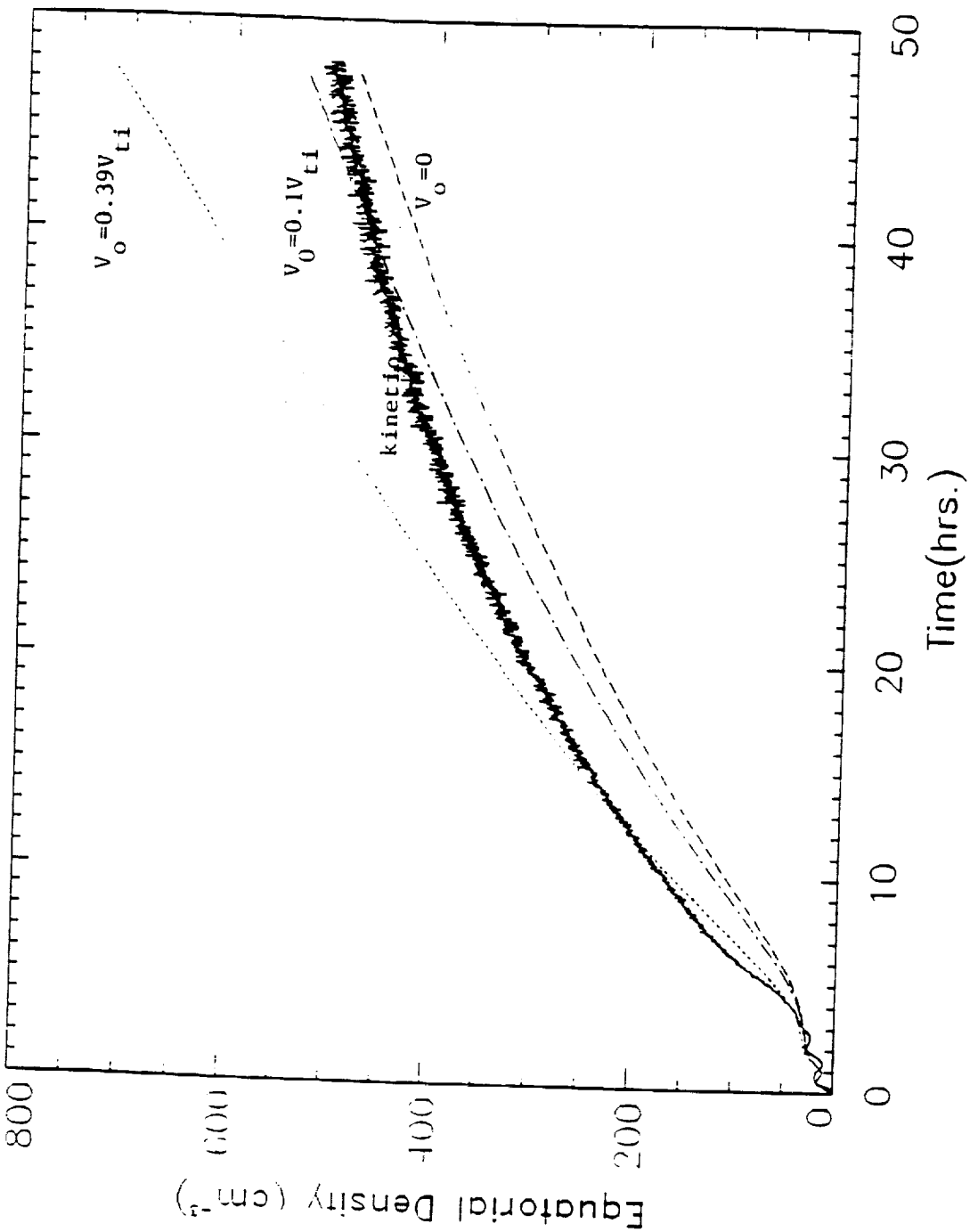
Equatorial Density (cm⁻³)
800
600
400
200
0
0
10
20
30
40
50
Time(hrs.)
$v_o=0.39v_{ti}$
$v_o=0.1v_{ti}$
$v_o=0$
kinetic

Fig. 10

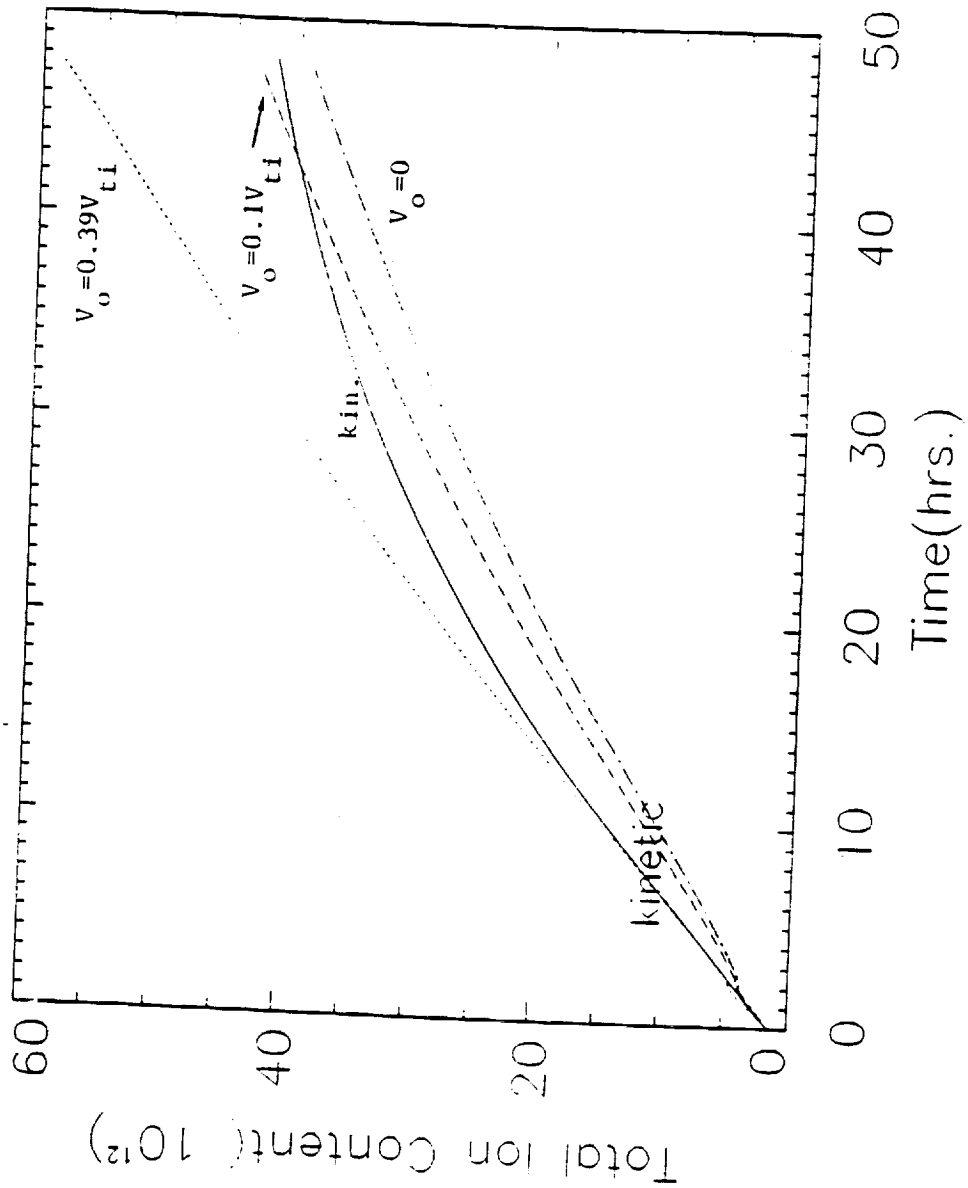
Total Ion Content ( $10^{12}$)
0
20
40
60
0
10
20
30
40
50
Time(hrs.)
$V_o$=0.39$V_{ti}$
$V_o$=0.1$V_{ti}$
$V_o$=0
kinetic

Fig. 11

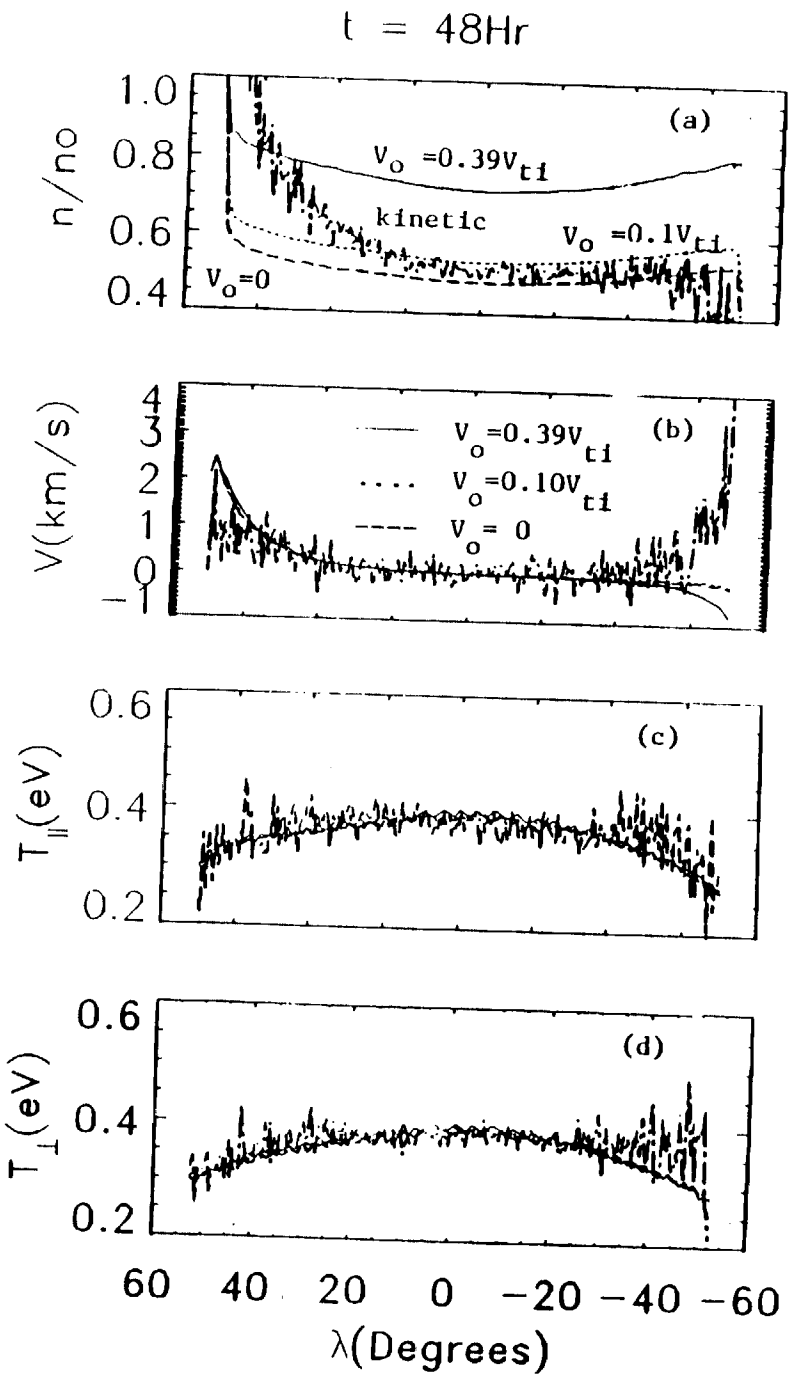
t = 48Hr
n/no
1.0
0.8
0.6
0.4
(a)
$V_o$ =0.39$V_{ti}$
kinetic
$V_o$ =0.1$V_{ti}$
$V_o$=0
V(km/s)
4
3
2
1
0
−1
(b)
$V_o$=0.39$V_{ti}$
$V_o$=0.10$V_{ti}$
$V_o$= 0
$T_{||}$(eV)
0.6
0.4
0.2
(c)
$T_\perp$(eV)
0.6
0.4
0.2
(d)
60 40 20 0 −20 −40 −60
λ(Degrees)

Fig. 12